MULTI-INK 3D PRINTING OF UV-CURABLE SILICONES

MULTI-INK 3D PRINTING OF UV-CURABLE SILICONES

By MICHAEL ZLATIN, B.Sc.

A Thesis Submitted to the School of Graduate Studies in Partial Fulfilment of the Requirements for the Degree Master of Applied Science

McMaster University MASTER OF APPLIED SCIENCE (2018) Hamilton, Ontario (Engineering)

TITLE: Multi-Ink 3D printing of UV-curable silicones AUTHOR: Michael Zlatin, B.Sc. (McMaster University) SUPERVISOR: Professor Ponnambalam Ravi Selvaganapathy NUMBER OF PAGES: vii, 80.

Acknowledgment

I would like to express my deep gratitude to Professor Ponnambalam Ravi Selvaganapathy, my supervisor, for his guidance, endless patience and encouragement. I would also like to express my very great appreciation to Professor Mike Brook for the creation of this project and for all the advice and support throughout.

I would like to offer my special thanks to my collaborator, Sijia Zheng, for her half in this research and for her cheerful company in many late night experiments.

I would also like to extend my thanks to the technicians of the machine shop of the mechanical department, Mark Mackenzie, John Colenbrander and Michael Lee for their help in making the printer.

I would like to thank the entire CAMEF lab group, for all their help and great company over the last two years.

I would like to thank the friends I have made at McMaster, which really made the last two years unforgettable.

Finally, I would like to thank my family for supporting me on this adventure overseas.

Abstract

Silicones are an important implant material, and as additive manufacturing technologies are revolutionizing many fields, one interesting application is the production of patient-specific silicone bio-implants where the stiffness of the material may not be homogenous over the entire part. 3D printing technology is well suited for construction of such custom parts. However, current 3D printing methods for silicone are not capable of printing multiple materials to mimic the heterogeneous properties of real tissue. The objective of this thesis is the development of additive manufacturing method for silicone objects with multiple constituent inks. To this end, a pneumatic 3D printer to print multiple silicone UV-curable inks based on thiol-ene chemistry was developed. The effect of parameters such as nozzle diameter, applied pressure, feedrate and Z offset on the ink deposition process was investigated and optimized printing conditions determined. The results showed that a successful creation of a continuous ink trace depends on correlating these parameters, a simple model for this correlation is presented. By optimizing parameters, traces of 600µm in width and 80µm in height were produced. Another key factor for the trace dimensions and for preventing clogging failures was found to be the UV illumination pattern in the vicinity of the nozzle. By optimizing exposure, continuous printing for 30 mins was demonstrated. The complete system was shown capable of printing 3D objects composed of three different silicone inks with capabilities such as disconnected feature printing, printing of overhangs and two modes of ink switching. Such a printer can be potentially applied in the fabrication of custom implants, production of meta-materials and bio-printing.

Terminology

$\boldsymbol{P}$ - Pressure

$\boldsymbol{Q}$ - Flowrate. In the context of deposition, it is defined with respect to the needle opening.

F - Nominal feedrate, the movement speed of the printhead during printing.

$\boldsymbol{Z_0}$ - Z offset, the distance between the tip of the needle and the substrate -in the

Trace - A single continuous connected deposited line of cured ink. The printer draws the object in such traces which can be part of layers or stand by themselves.

Trace height - The height of a single printed trace. Measured from the previous trace or the printbed, up to the highest point of the trace.

Trace width - The width of a single printed trace. Measured from the extreme one side of the trace to the other when looking from the Z direction.

$\boldsymbol{AR}$ - Aspect ratio, the ratio of the height to width of the trace, Dimensionless.

first layer it is the printing bed, in the subsequent layers it is the previous layer

$\boldsymbol{\mu}$ - The ink viscosity

Outline

1.Motivation and Organization

3D printing is an emerging technology that is poised to complement, and in some cases supplant, the current methods of manufacturing and enable new structures, material combinations and functionality. It is defined by the ASTM -an international standards organization, as "*The fabrication of objects through the deposition of a material using a print head, nozzle or another printer technology*" It is a form of fabrication of various objects, where the object is built up layer by layer from the design of the 3D object drawn using a CAD software. This form of manufacturing is in contrast to traditional machining where the final form of the object is obtained by machining away or a bulk stock using a removal tool. A number of additive manufacturing methods have been developed over the last decades. They can broadly be classified into two categories.

1. Selective spatial fusion/bonding/sintering of a 'fluid' stock such as powder or liquid resin that is spread over the entire print bed as a thin layer so that only the regions constituting the part is "solidified" or binded. This group includes such processes as stereolithography (SLA), selective laser sintering (SLS), and binder jetting
2. Selective deposition methods, where the object is built incrementally from a printhead delivering ink material along a path that fills the constituting parts of the object. This group includes such processes as fused deposition modelling (FDM) where the ink is a thermoplastic filament, or direct writing (DW) where the ink is a pre-polymer liquid that can be solidified by polymerization.

3D printing is resource efficient and is practically waste free. It does not require tooling, allows single and small batch manufacturing without the typical costly initial setup overhead required in traditional manufacturing such as machining or

injection molding. It enables fabrication of objects and shapes which are not possible by other traditional manufacturing processes. And it can potentially allow integration of multiple materials with varying properties into a single fused object.

Silicones, first named in 1901 by Frederick Kipping are a group of polymers with a siloxane (Figure 2.1) backbone chain. Silicone elastomers -a solid form of crosslinked silicone- have some very useful properties, they are non-toxic, exceptionally stable chemically, excellent thermal and electric insulators and bio-inert. These properties make it suitable for many applications in diverse fields such as implants, electronics, consumer goods, automotive marine and aerospace parts, industrial machinery, medical parts and others. The silicone market is projected to reach 7.9B$ by 2021[34].

Typically, silicone parts are manufactured using traditional molding methods, such as injection molding, or casting. These methods while suited for mass production have a prohibitive set up overhead for small scale, prototyping or customized manufacturing. These are precisely the areas of manufacturing where 3D printing excels. Therefore, development of a method to 3D print silicones as well as suitable inks would be very valuable for prototyping, custom and small batch fabrication.

Furthermore, traditional manufacturing methods allow fabrication of parts and components that are made of a single material. Assembly of different parts machined using different process may need to be made to obtain a multi-material combination. In addition, incorporation of gradually varying properties within a single part will be difficult. However, in many applications, it would be highly desirable to have a single object composed of a multitude of materials. One such application is the fabrication of customized implants with different stiffness in

various regions to mimic natural human parts. For example, a human ear cartilage is stiff on top and soft at the lobe area. Presently there are no viable way to fabricate such an implant which would exhibit both properties in a single fabrication step.

Another example would be a breast implant, especially for women who have undergone a mastectomy. In this case, it would be highly beneficial to the patient to have a custom 3d printed implant which mirrors the other breast in both shape, softness and its distribution. Currently, such a patient only can choose from a limited set of mass produced implants.

Therefore, this thesis focuses on the development of an AM technology that can print 3D structures using silicone inks. It also focuses on developing capabilities for multi-material printing.

The thesis is organized as follows:
Chapter 2 - presents an overview of 3D printing of silicone and a literature review of current efforts in the field
Chapter 3 - provides information on the materials and methods used in this thesis and discusses the design of the common parts that are used in later experiments
Chapter 4 - discusses in detail the design of the printer, its parts and their integration
Chapter 6 - covers the characterization of the material deposition process as well as systematically determines the influence of each of the control parameter on the printed trace.
Chapter 7 - provides several examples of printed structures that illustrate the various capabilities of the printer
Chapter 8 - provides a conclusion of the thesis and proposes future work.

2.Introduction

2.1.Silicones

Polysiloxanes or silicones are synthetic polymers of repeating siloxane (figure 2.1) backbone chain. Since the -Si-O- backbone structure is inorganic, silicones are a type of inorganic polymers. With a general formula of $[R_2SiO]_n$ where R is typically an organic group such as ethyl, methyl or phenyl. Silicone molecules come in three forms: 1) cyclic-where the polymer is in a form of a ring, 2) linear-a chain of varying length and 3) crosslinked-a macromolecule of interlinked chains.

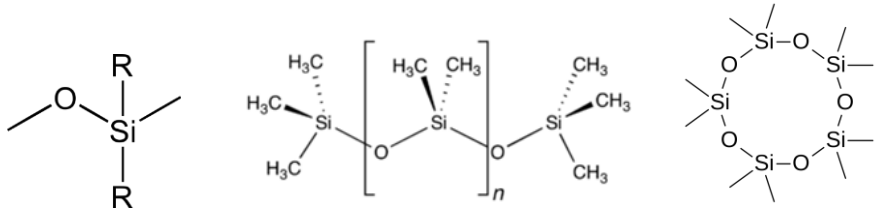

Figure 2.1, Siloxane, the building block of Silicones (Left), Polydimethylsiloxane a linear silicone and the most common of silicones (center), Decamethylcyclopentasiloxane, a cyclic silicone (right)

The Si-O bond is highly flexible, allowing free rotation of the silicone molecule, which translates into a very low glass transition temperature and also the resulting elasticity of crosslinked silicone solids. For instance, Sylgard 184 PDMS has a glass transition temperature of ~-125C° and has an elastic modulus of 1.32–2.97 MPa[32]. Further, the bond is heat-resistant and remarkably chemically stable.

Silicones can come in a variety of forms: liquid, gel, resin and solid elastomer, depending on the respective molecular weight and degree of crosslinking. Low molecular weight uncrosslinked silicones have wide application as lubricants, hydraulic fluids, water repellent coatings and electrically insulating varnishes and oils [28]

Figure 2.2, The many uses of silicone rubbers, left to right, tubing, a molded medical device, robotic gripper, extending auto seal, RTV sealant, gasket, breast implants, finger-joint implant, contact lens, electronic encapsulation, flexible keyboard, consumer products.

Crosslinked high molecular weight silicones form elastomers or synthetic rubbers. The excellent physiochemical properties of silicone elastomers such as its thermal and chemical stability, optical transparency [12], gas permeability [13] chemical inertness and low environmental impact [14] to name a few have led to its adoption in various fields of science, medicine, engineering, consumer products, construction and industry (see figure 2.2).

In the medical fields, silicone elastomer’s bio-compatibility [11] make them the most commonly used materials for soft human body implants [15] such as breast, testicular, pectoral, finger-joint [29], contact lenses and other areas of the body where its mechanical similarity to cartilage and soft tissue and its bio-inert properties are desirable.

In molding applications, the flexibility and low surface energy of silicone rubbers make them suitable as an excellent mold material for resins, foams, concrete and other rubbers, as they typically do not require a mold release agent. In construction, one-part moisture cure RTV silicone sealant caulks are broadly used for general sealing applications.

In the machinery and industry, silicone elastomers are used in gaskets, seals, piping and tubing, and many other flexible parts subjected to harsh conditions. Silicone's excellent electrical resistance makes them useful in electronics. Silicone potting formulations are used to protect electronic components and as coatings for solar cells.

Polydimethylsiloxane (PDMS), a variety of silicone has found widespread use in emerging scientific fields such as microfluidics [16], as scaffolds for cells [17], flexible electronics [18] and as gas permeable membranes [31] due to its ease of molding, optical properties and nanometer scale feature replication [30].

There are three routes for the crosslinking of silicone prepolymer systems. Each route requires the right combination of curing agents, catalyst and side groups on the polymer.

Moisture cured silicone is a type of condensation cure, it is supplied as one part in a sealed container. Upon exposure to the atmosphere, the ambient moisture hydrolyzes the cross linker and functional groups on the base polymer which then condense and cure the rubber. This mechanism typically produces undesired volatile by-products. Since the cure rate depends directly on the available humidity, it can be hindered by dry environments. In addition, since the cure initiates from the surface and proceeds into the bulk by diffusion of moisture into the material, the depth of cure is limited as well to typically less than 10mm. Cure time is on the order of hours and it cannot be accelerated by heating. This curing mechanism is used in silicone sealants as no further steps are required after application.

Thermal cure or high temperature vulcanizing (HTV) can come as one or two-part system and is a type of addition cure using a platinum catalyst. This reaction does

not produce by-products or shrinkage of the final shape. Two-part systems can be designed to cure at room temperature as well, while one-part system require heat to initiate the reaction. Application of excess heat accelerates the reaction.
This curing mechanism is often used in injection molding of silicone products.

Photo cure, uses light to initiate the crosslinking reaction. Typically, ultraviolet light is used due to its energetic photons to break apart a photoinitiator molecule and initiate the reaction. It is a one-part system stored in a dark container prior to usage. As the reaction is completely controlled by the light flux, to achieve full cure, the entire part requires adequate illumination while shadowed areas will not cure. This cure mechanism is well suited for coatings and optical components.

2.2.Additive manufacturing

Since the introduction of 3D printing by Chuck Hull in the 1980s, the world of Additive manufacturing (AM) has expanded into a myriad of technologies. Currently, the ISO/ASTM 52900 standard defines seven broad process categories of additive manufacturing.
In binder jetting, a liquid bonding agent is selectively deposited to a thin layer of a building powder material. New powder material is introduced between successive layers as the part is built up. Binder jetting can utilize diverse building material such as metal, ceramics, plastics in powder form, glass and sand. A post processing sintering step is added for metals and ceramics to fuse the particles. It is a comparably rapid process.

In directed energy deposition, build material in the form a wire or powder is fed into a material melt pool, which is generated on the surface of the part by an energy source such as laser or an electron beam. It can be seen as a form of additive welding. It can be used for the creation of new parts as well as repair or build-up of existing parts. It allows incorporation of multiple materials into a

single part. Additionally, it is not limited in the build direction as other methods. The typical build material is metal wire, powder or ceramics.

In powder bed fusion, powder material in a build vat is fused by the application of a directed thermal energy such as electron beam or a laser. It is similar to binder jetting, but whereas in binder jetting the fusion is by bonding, in powder bed fusion it is by melting. The process affords a high level of complexity and can utilize powder metal, plastics and ceramics.

In sheet lamination, separate sheets of material forming two dimensional slices of the printed object are cut from a roll. The layers are stacked sequentially and bonded to form a single object. The bonding can be achieved by adhesive, or by physical methods such as ultrasonic bonding. It can be used with paper or plastics film or with metal foils. It is a comparably cheap process with high build rates but low resolution.

In vat photopolymerization, a liquid resin housed in vat is selectively cured layer by layer by light-activated polymerization which turns the liquid into a solid in the exposed areas. The light can come from a laser source which traces out the layer or by a digital mirror array which exposes the entire layer at once. The process allows high resolution and complexity with a smooth surface finish.
It utilizes photocurable polymer resins.

In material jetting, droplets of a build material are selectively deposited to form an object. The droplets can be of photocurable polymers which are deposited and subsequently exposed or droplets of molten material which then cool and solidify. The process enables high resolution, incorporation of multiple materials in a part and full color parts. It utilizes waxes, photopolymers or thermoplastics.

In material extrusion, build material is selectively deposited as drops or traces through a nozzle to build the object layer by layer. In fused deposition modelling, a form of extrusion, the material is a thermoplastic filament which is molten at the nozzle and solidifies once deposited. In direct writing extrusion, the material dispensed is a liquid or a paste which then cures via a number of possible routes such as photocure, thermocure, solvent evaporation and others.

2.3.Silicone 3D printing

As silicone is an important industrial material, recent effort has been undertaken to additively manufacture 3D objects in silicones. Silicones are particularly suitable for three types of additive manufacturing: Vat polymerization, Material extrusion and Jetting.

2.3.1.Silicone vat polymerization

Stereolithography is a form of vat photopolymerization that is often used for 3D printing of silicones. This approach has been adapted to silicone by Femmer et al [1] who have used a commercial DLP-SLA printer and an ink consisting of a mixture of silicone prepolymer, photoinitiator and an absorber dye to 3D print objects. The photoinitiator starts the radical polymerization reaction in the places that have been exposed to light and the absorber dye is used to limit the unwanted spread of curing. With a reported resolution of $300\mu m$, they have been able to 3D print complex silicone objects. However, the curing time for a single $100\mu m$voxel is 12s. Also, with the use of the absorber dye the optical transparency of PDMS, which is useful for many applications, is lost. To achieve lower resolution Rekštytė et al [2] have used a femto-second laser with a small spot size instead of a digital micromirror display. They have been able to 3D print micro structures with a reported resolution of ~$5\mu m$., However, this is a single spot technique and the laser must raster through the entire layer to define it. They report a volumetric build rate of $720\mu m^3/s$. Carbon3D, a maker of SLA printers

has adapted a silicone-urethane copolymer for their printer which offers rapid build rates of 25 faster to traditional SLA using their continuous layer interface [14] with 75µm resolution. Vat photopolymerization is suitable for silicone, due to its liquid prepolymer state, however silicone's transparency in most wavelengths [11] presents unique challenges which were solved either by the incorporation of the dye as in [1] or by use of very focused laser as in [2], or the use of a copolymer as in [14].

2.3.2.Silicone extrusion

The other approach that is commonly taken in silicone 3d printing is material extrusion also known as direct writing. Silicone, being a material with typically long curing times presents a challenge in the application to extrusion. Liravi et al [3] have used a commercial deposition system with a viscous photocurable silicone ink to fabricate 2.5D shapes with a resolution of ~400µm. Moisture cure silicones have also been extrusion printed. Structur3d, a Canadian company developing extrusion printers [7] have demonstrated 3D printing of commercially available moisture cure RTV silicones with a resolution of ~800µm. Similarly, other syringe dispensing printers such as Hyrel™ operate on a similar principle of dispensing moisture cure RTV silicone. Using silicones of high viscosity, whether RTV or photocurable enables the extruded filament to hold its shape while being cured. However, it also results in a rough surface and poor adhesion between individual layers. Additionally, due to the high pressures required to dispense them, there is typically a time lag for the pressure to build up, which negatively impacts printing of more complicated parts that require rapid control. Wacker Chemie AG [6] have developed a drop-on-demand printhead for silicone droplet jetting with UV cure, and a resolution of ~400µm. However, the ink is expensive at about 10$ for 1ml.

One solution to maintaining desired geometry during printing of low viscosity silicone inks is the use of a support material. Hinton et al [4] have used a carbopol gel as a support medium to 3d print common SYLGARD 184 with a long 72h cure time. The support gel behaves as a Bingham plastic during the print process. O'Bryan et al. [5] improved on the method by utilizing a self-healing microgel with unique thixotropic rheological properties as a support medium for the deposited silicone ink. This method utilized the jamming behavior of the microgel to constrain the movement of the ink following extrusion, allowing the trace to cure in place with a reported minimal resolution of $300\mu m$for a single trace and ~1mm for a single wall object. While a support medium method allows the fabrication of 3d objects with slow curing low viscosity ink, it increases the complexity and number of pre and post processing steps required.

In terms of resolution, light polymerization technologies such as SLA are better, as the feature size is limited by the spot size and light dispersion which can be as low as$5\mu m$ as shown by [2]. In comparison, the resolution of the extrusion based approaches are limited by the size of the extrusion needle to hundreds of microns. Furthermore, large pressure gradient is required to extrude the viscous silicone ink through the nozzle. Extrusion methods, however, have a faster build rate as compared to SLA and allow the fabrication of larger objects in the centimeter scale, as shown in [5][7]. Additionally, multi-material printing is possible only in extrusion type printing.

A significant requirement of any extrusion technology to qualify as 3D printing is the ability to rapidly control the state of the ink flow, to enable, without significant time lag to start and stop a steady flow of build material. This 'stop and go' extrusion capability is required as any printed part of a nontrivial geometry will have multiple individual traces that make up a single layer. For example, a layer with disconnected features will necessarily have travel moves

between them. In traditional thermoplastic FDM deposition, the filament mechanical drive provides immediate response to control to actuate extrusion. However, syringe pumps which are commonly used in silicone extrusion such as in [7][4] have a response lag depending on the fluidic path to the printhead and the overall hydraulic capacitance of the system, limiting them to shapes which can be sliced without many travel moves.

2.3.3.Multi-ink 3D printing

Multi-ink printing is the next frontier in 3D printing. It enables incorporation of a number of different materials with potentially different mechanical, optical or chemical properties into a single object. This provides capabilities for fabrication that were not possible before. Advanced bio-printing, for example, requires the use of an array of inks loaded with different cells. Future custom-made bio-implants must incorporate materials of varying properties, as a single material can never capture the exact constitution of complex human tissue. Multi-ink printing is fundamentally limited to selective deposition 3D printing processes, such as extrusion or jetting. Selective fusion, bonding and polymerization processes are inherently limited to a single material. Because the object is necessarily being printed out of a single homogenous build volume.

Multi-ink 3D printing has been available for some time in traditional FDM 3D printers such as RepRap by simply multiplying the number of installed printheads on the printer. Similarly, low cost multi-material bioprinters have also been developed [8][9] using the same approach. Hardin et al [10] have developed a dual material printhead for silicones, with one tip driven by two simultaneously controlled syringe pumps. However, due to the hydraulic capacitance of the system, resulting from the compliance of the flexible tubing, this method requires

complex control of both pumps and does not scale well to more than two materials.

The common architecture of multi-material printers, however, incorporates multiple printing tips. Such scaling is inherently limited in the number of possible materials, as each additional tip competes for valuable printhead space. The accuracy of such printers is also lower than single tip printing, as the actual offset between the tips will inevitably vary from the programmed one, resulting in misalignment in the printing. More importantly, multi-tip printing proves untenable for rapidly photoreacting inks. As residual ink in the inactive print tips gets exposed to curing conditions and clog while idling.

Although significant advances have been made in the 3D printing of silicones, there are limitations to many of the established approaches. An ideal 3D printing system will solve the challenges of maintaining geometric fidelity of the fluid ink during curing while enabling rapid build rates competitive with other 3D printing methods. It will also provide rapid flow response to enable true ‘stop and go’ printing. Finally, it should enable scalable incorporation of multiple ink 3D printing.

3.Materials and Methods

3.1.Materials

Throughout the research, various inks have been used. They can be classified into thermal and UV curable inks. Commercially available Sylgard 184 [20] was used as the only thermal ink, while many custom formulations prepared by a collaborating group were used as UV curable inks.

Thermal cure ink: The thermal ink 'Sylgard 184' was purchased from 'Dow corning'. It is a platinum-based heat curing two-part silicone compound, manufactured for potting electronics and solar cells. Before usage, it is mixed in a ratio of curing agent to base of 1:10. The mixed product has a viscosity of 3500 cSt and a pot life of 1.5 hours. Its cure is greatly affected by temperature. For instance, at 25C° it will cure in 48hrs, and at 100C° in 35 min.
However, it was found to harden enough to hold its shape in a less than 10s when extruded in 1 ml droplet volume onto a 110°C surface. Once cured it is has a tensile strength of 6.7MPa [20]

UV curable inks: There are various UV curable silicone chemistries. In this thesis UV inks based on the thiol-ene 'click' reaction were used. These inks were custom formulated by adding a base, a crosslinking group, a chain extender and a UV photoinitiator. The curing is generally based on the principle of free radical crosslinking, where the free radical is a semi-stable initiator molecule with an unstable bond which breaks apart into one or more radicals when illuminated with UV light of the appropriate wavelength. Common photoinitiators such as 2-hydroxy-2-methylpropiophenone [22], that have been used with silicones as in [21] and [2] have absorption peaks around ~250 nm (UVC). However, emission sources in this wavelength are difficult to obtain and are expensive.

Alternatively, phosphine base photoinitiator such as 'Irgacure™ TPO-L' [24] (Ethyl (2,4,6-trimethylbenzoyl) phenylphosphinate-sold by BASF) can also be used [1][2]. Fig 3.1.c shows the structure of the photoinitiator.

These photoinitiators are excited at longer UVB wavelengths, with a secondary peak at 380 nm. This photoinitiator was found to cure the thiol-ene click chemistry reactions used in this research very rapidly in simple proof of concept experiments.

The UV source that could be used to initiate the reaction should be a strong UV source such as a metal halide lamp, which produces a broader spectrum UV, with peaks distribution typically between 300nm-400nm (varies by lamp design and filtering). An 'S1000 Omnicure' [23] curing system from 'Lumen Dynamics' (elaborated in printer design) which provides a wide spectrum UV of up to 100W with two lightguides which produce a narrow cone of ~30° was used as the light source.

3.1.1.Thiolene inks

The thiol-ene inks have been developed and optimized for the purpose of 3D printing by our collaborators. The thiol-ene reaction is an organic reaction between a thiol and an alkene (in our case a vinyl group). One part of the reaction is a silicone copolymer of mercaptopropyl-methylsiloxane (the thiol) and dimethylsiloxane monomers (fig 3.1.a). The other part is vinyl terminated silicone chains (fig 3.1.b).

The thiol-ene 'click' reaction happens between the vinyl and the thiol groups, crosslinking the ink. By varying the ratio of the thiopropyl groups and the molecular weight of the vinyl capped chains, the crosslinking density can be varied and with it the elasticity of the resulting elastomer.

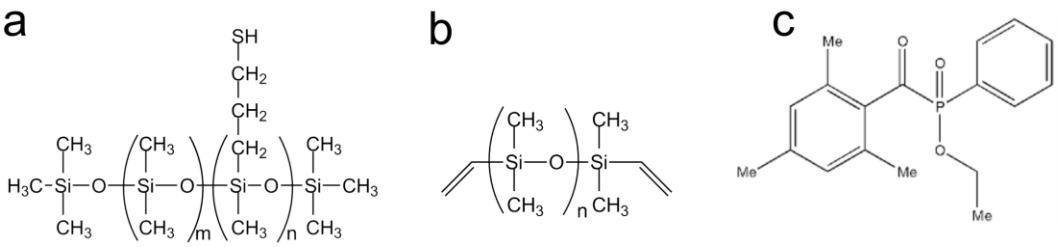

Figure 3.1, a) Silicone dimethyl thiopropyl copolymer, aka sms-142,sms-022 b) Vinyl terminated PDMS c) Ethyl (2,4,6-trimethylbenzoyl) phenylphosphinate, Aka TPO

Thus a few components[1] were employed in the inks used.

1. Vinyl terminated PDMS chains of varying molecular weights (fig 3.1.b)
2. SMS-142, The thiopropyl copolymer where the ratio of thiopropyl residue to dimethyl residue is 13%-17%, acts as a crosslinker (fig 3.1.a)
3. SMS-022, The thiopropyl copolymer where the ratio of thiopropyl residue to dimethyl residue is 2%-3%, acts as a chain extender (fig 3.1.a)
4. AEROSIL-150 fumed silica, acts as a reinforcer and a thixotropic agent in some inks
5. TPO-L photoinitiator (fig 3.1.c).
6. Silc Pig[2]. silicone pigments

Various inks with different properties were formulated (by our collaborating group) by mixing these constituents in different ratios as shown in Table 3.2. 'TPO-L' and 'Silc Pig' are not listed, as they were varied across experiments. Typically, the concentration of Silc Pig was <1%.

Table 3.2 Optimized formulation for 3D printing inks

[1] The silicone components were provided partially as in kind contribution from our industrial partners.
[2] Purchased from SmoothON™

Inks	Vinyl terminated PDMS MW(g)	SMS-142 mol% (g)	SMS-022 mol% (g)	AEROSIL-150 wt%(g)
function	Base	Crosslinker	Chainextender	Reinforcing agent
V21H	3,850(10.00)	100(8.54)	0(0.00)	2(0.37)
V21S	3,850(10.00)	10(0.43)	90(16.30)	2(0.53)
V31H	21,500(10.00)	100(1.52)	0(0.00)	0(0.00)
V35H	42,300(10.00)	100(0.77)	0(0.00)	0(0.00)

3.1.2.Extrusion needles

Flowrate depends strongly on the needle diameter, as shown by equation 3.1 derived from the Hagen Poiseuille equation.

$$Q = \frac{\Delta P \pi \mathrm{D}^4}{128 \mathrm{L} \mu} \tag{3.1}$$

Where L, D are the corresponding needle length and needle diameter for the needle gauge, μ is the fluid viscosity, and $\Delta P$is the pressure gradient.
Thus, needle diameter has the most significant effect on flowrate. Additionally, the needle diameter dictates the lowest resolution possible. It would be desirable to reduce the needle diameter as low as possible to achieve the highest resolution. However, that comes at the expense of flowrate, which prolongs the total print time. Hence the needle diameter selection is a trade-off between resolution and print time.

To select the needles, 3500 cSt (the viscosity of SYLGARD-184) was used as the reference viscosity and a pressure supply of 90 psi as the maximum pressure. Two needle gauges were chosen, 22Ga and 25Ga. The 22Ga needle covers flow range of $0\frac{ml}{min}$ to$0.5\frac{ml}{min}$ and the 25Ga for flow range of $0\frac{ml}{min}$ to $0.1\frac{ml}{min}$. Even though both needles can work in the $0\frac{ml}{min}$ to $0.1\frac{ml}{min}$ range, the 25Ga provides a

finer control of the flowrate and offers higher resolution. The needle length was the shortest commercially available at ¼". And all the needles were purchased from Aliexpress™ and McMaster-Carr™

The needles were measured using light microscopy and image analysis with ImageJ [26] and to estimate their true dimensions, provided in table 3.3.
The experimental ID was averaged from 4 samples with two standard deviations provided as the error bound

Table 3.3, True needle dimension

Needle gauge	22Ga	25Ga
Nominal ID [μm]	413	260
Experimental ID [μm][3]	430 ± 10.1	280 ± 20.2

3.2.Methods

3.2.1.Flow rate measurements

Flowrate measurements were conducted with a simple setup. A 10ml syringe barrel (McMaster Carr™) was connected to a controlled pressure source (either automatic or manual). A needle or a printhead with a needle were attached to the syringe barrel by its luer lok connection. A standard weighing dish (whose weight was measured before) was used to collect the ink flow over the specified time. At which point the pressure was removed to immediately stop the flow. Without the application of pressure, the gravity induced flow was minimal. Usually, a drop forms at the tip of the needle and accumulates until any residual flow completely

[3] Measured from 4 samples via light microscopy and pixel distance calculation on the extreme tip of the respective needle.

stops. The dish was then weighted with standard lab scales (resolution of 0.01g) and the results logged.

In order to measure the density of the inks, a graduated cylinder was used to measure a precise volume of the ink and weighed. In cases where sufficient quantities of ink were not available, a value of 0.96ml/g (measurement made by collaborators) was used to convert mass to volume.

3.2.2.Characterization of the shape of printed line

In order to characterize the shape of the printed line, it was sectioned and imaged from the side. Initially, an ink trace was printed according to the desired specifications on a thick 6mm flexible and transparent PVC tape (McMaster Carr™). Multiple such lines were drawn on a single substrate under several flow and feed rate conditions. The spacing between the lines was fixed at 2mm[4]. The substrate was removed from the printer and cut into strips perpendicular to the line direction, then the strips were attached to a 90° holder and imaged under a microscope with strong bottom illumination.
This produced a sharp silhouette of the printed trace (figure 3.6a) and the printed PDMS and the polymer substrate could also be clearly differentiated from each other. From this image, parameters such as the height, width and the shape of the trace formed were extracted.

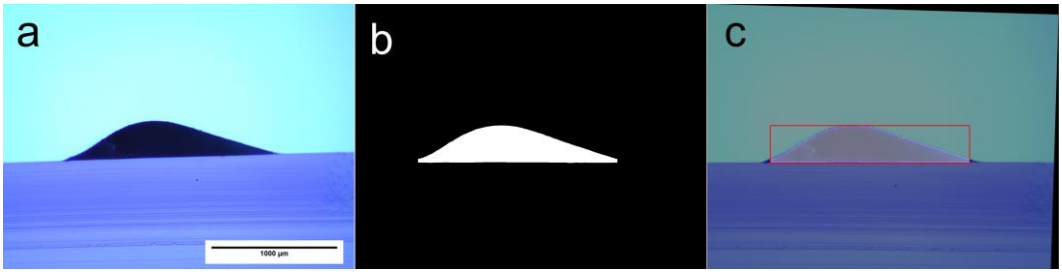

[4] The 2 mm spacing is required to have a single trace per microscope capture

Figure 3.6. a) An image of a single printed trace cross section on a glass slide, made using the trace sectioning procedure. b) The isolated section area c) a composite of the input from a and b, along with a box enclosing the recognized section

Automated image processing was done on these images to extract the parameters of interest. A computer vision script was written for Python 2.7, Using NumPy and OpenCV [25]. The details of the algorithm are provided in appendix B. Images as shown in figure 3.6.a were used as the input. The script performed automatic rotation to level the substrate, performed edge detection and performed background subtraction to isolate the shape of the trace as shown in Figure 3.6.b. The output was the rotated and leveled image as shown in figure 3.6.c as well as the computed trace height, width and area.

4.Printer design

Currently, typical extrusion printers are able to print only one type of ink at a time. Multi-nozzle printers can be used to print multiple inks but require precise alignment accuracy to ensure that the regions printed with different inks will align with one another. Furthermore, smooth transitions between the different regions with inks also are difficult to achieve. Therefore, a new approach where multiple inks can be routed through a single nozzle and the sequence of the ink dynamically controlled was developed. An ideal printer for such purposes must be able to switch the ink flow rapidly to enable precise deposition without time lag. It must be reliable and allow clogging free operation. It must be able to rapidly cure the deposited ink. It must allow synchronous control of movement, illumination and deposition.

4.1.Design considerations

4.1.1.Hydraulic capacitance

The Hydraulic capacitance is defined in analog to electric circuits as $\frac{dV}{dP}$

The overall hydraulic capacitance of the printhead is the major factor influencing the rate of response of the system. Specifically, hydraulic capacitance increases the lag time between the actuation command and establishing steady state deposition flow. The lag is similar for stopping of the flow and for switching of inks. The lag is resulting from the time required to equilibrize the pressure while the complaint parts of the system expand to take a part of the fluid volume.
A significant source of hydraulic capacitance comes from elastic and flexible components in the printhead such as tubes.

The length of the fluidic path also contributes both to the hydraulic capacitance due to some compressibility of the fluid as well as the hydraulic inertness of the fluid mass. Thus, to enable a rapid rate of response the total hydraulic capacitance of the system must be minimized. This can be achieved by minimizing the path between the ink reservoir and the nozzle, by using rigid components and by establishing operating procedures that minimize air bubbles.

4.1.2.Choice of fluid actuation method

There are a number of possible actuation methods that can be used to pump the ink through the nozzle in the flow range required ($1 - 50\ \mu l/s$). These include direct pneumatic pressure actuation or positive displacement pumps such as a syringe pump or a peristaltic pump. The design criteria to meet is maximizing the response rate of the system and enabling simple scalability of the system to multiple channels.

Peristaltic pumps are incompatible due to the high hydraulic capacitance of the flexible tubing and their pulsatile nature. Syringe pumps also have major drawbacks in this application. They are bulky and cannot be integrated directly into the printhead. Since a single unit is required per channel their application becomes expensive for scaling to multiple channels. Additionally, due to the tubing required to connect them to the nozzle, their response time can be large (on the order of 30s in our experiments).

Use of direct pneumatic pressure actuation, where the headspace above the fluid is directly pressurized was found to be the most suitable method for the printer. It is used extensively in industrial dispensing applications. It is not pulsatile. And its greatest advantage is that a steady state flow is established rapidly following pressurization. This is essential for rapid on/off control. It is also compact and suitable for scalability, its simplicity lends to the ability to offload much of the

actuation control parts to a location external to the printhead which enables miniaturization of the printhead itself and integration of multiple channels. Pneumatic direct actuation, however, requires calibration of the pressure to flowrate relation as the flow is not metered.

4.1.3.Actuation pressure

The choice of actuation pressure determines the maximum flow rate and rate of response. Higher pressure results in better performance characteristics. However, every pressurized component must be able to withstand that pressure. Excessively high pressure jeopardizes the safety of the system, as any loose connection is more likely to burst.

90 psi is a commonly used pressure for pneumatic applications. And all the components of the pneumatic system were rated for that pressure. Higher pressures would require significantly more expensive components. Additionally, 90 psi is a pressure which can be delivered in a portable format as well by a small tank or compressor. Thus, 90 psi was chosen as the maximum actuation pressure for the printer.

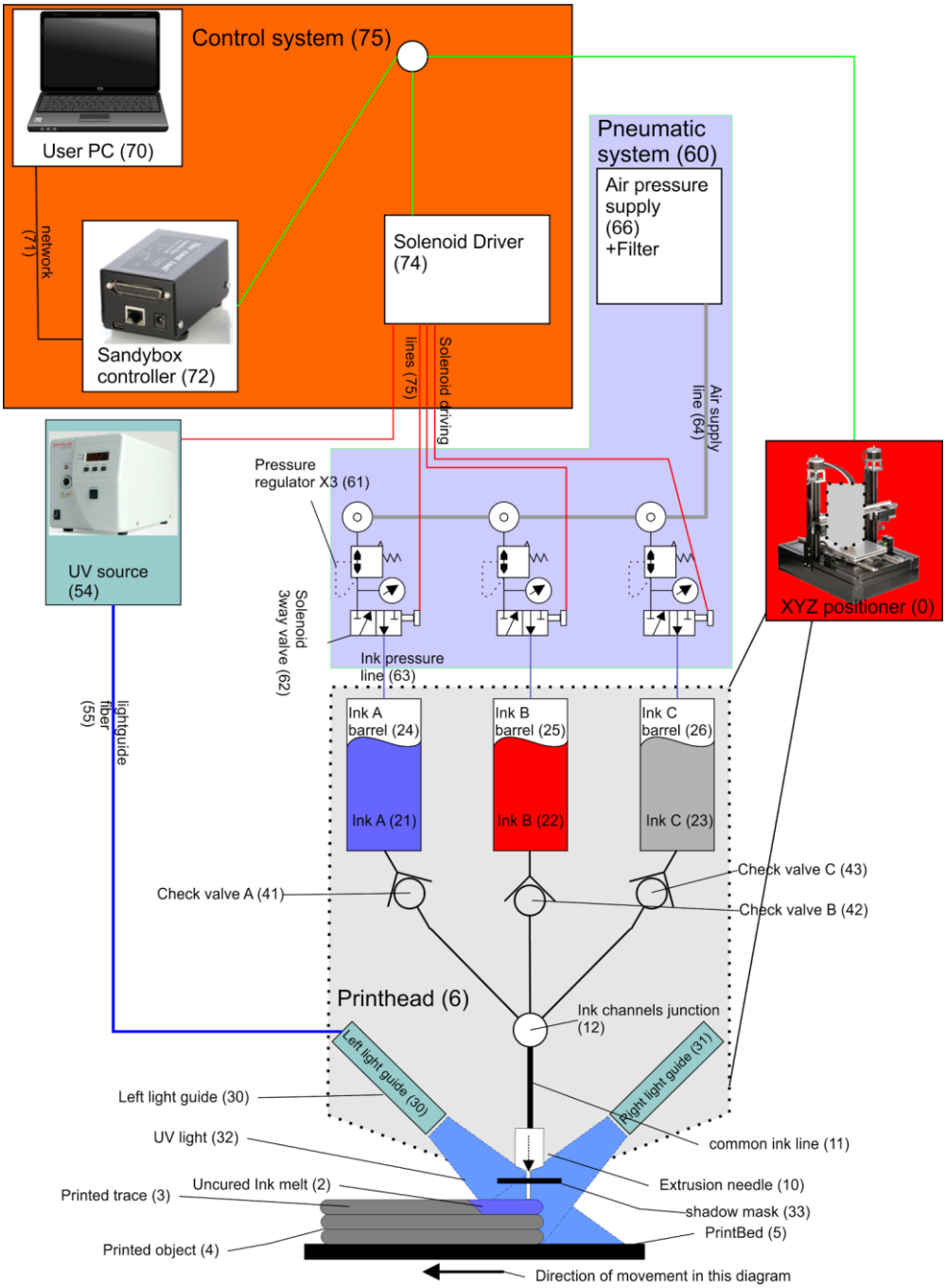

Figure 4.1, A schematic diagram of the printer components.

4.2.Printer design

The printer consists of an XYZ positioner (**0)**, a custom built multi-material printhead (**6**), a UV illumination system (**54**), a pneumatic control system (**60**) and an integrated computer control (**75**) to synchronize the movement of the printhead with the pneumatic system and the printhead's actuation (**62**)

The XYZ positioning system (**6**) was adapted from a commercially available UNI-PRINT-3D FDM 3D printer purchased from 'The Cool Tool' GmbH company. The original FDM printhead was removed and replaced by a custom designed printhead. This printhead is actuated by a pressure control system (**60**) external to the printer. A UV illumination system was used to initiate crosslinking in the extruded material. It consisted of an external UV lamp system (**54**) 'Omnicure S1000' that used two separate lightguides (**30,31,55**) that were attached to the printhead to route the light to the extrusion nozzle tip.
The printer, pressure system and UV lamp are controlled by a single controller (**75**).

4.2.1.Print head

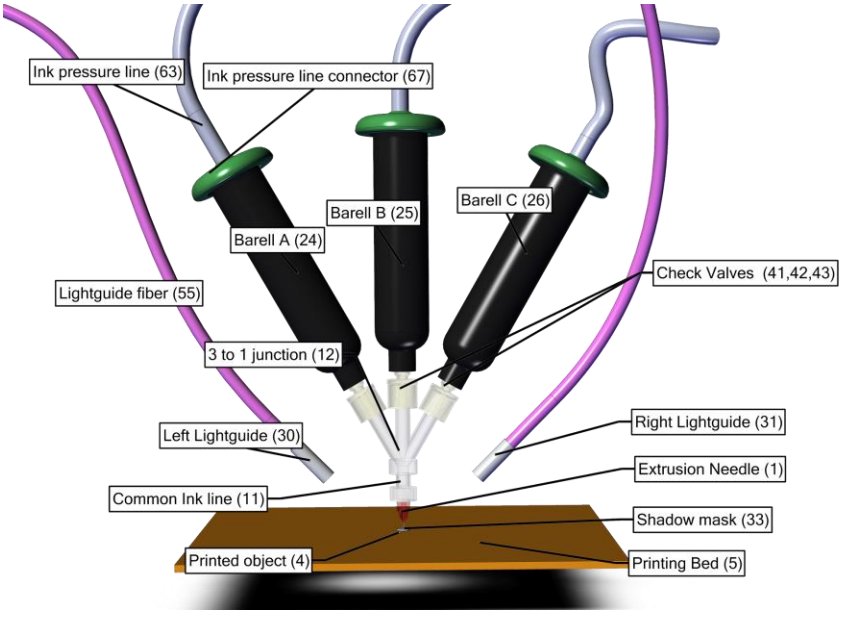

Figure 4.2, A CAD overview of the printhead

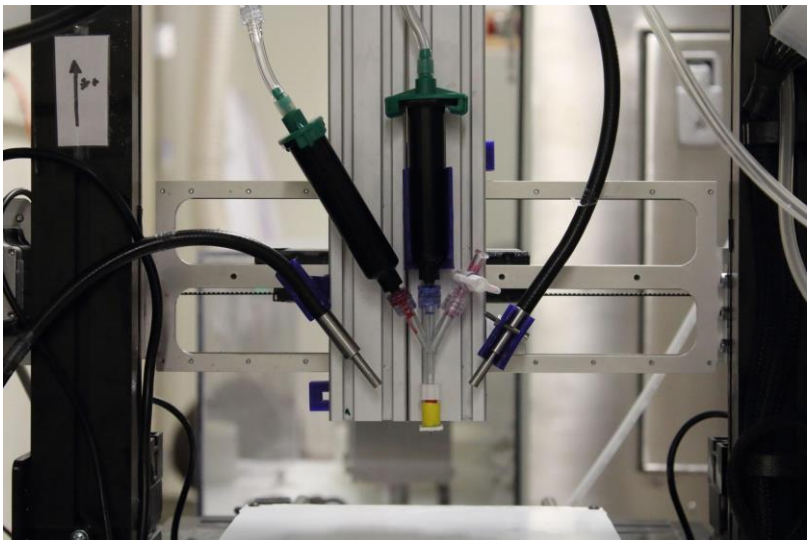

Figure 4.4, A photo of the printhead, the aluminum foil UV protection is not included for clarity, one of the barrels is replaced with an air purge valve.

The Printhead (**6**) consists of three barrels (**24,25,26**) that contain the inks (**21,22,23**) used in printing. The barrels were connected to a three to one junction (**12**) which was used to sequence the inks flowing into it with check valves (**41**,**42**,**43**) in between them to prevent any backflow of the inks. The outlet of the three to one junction leads to a dispensing nozzle (**10**) through which the ink was extruded out. Blunt tip ¼” needle 22Ga or a 25Ga needles were used as the dispensing nozzles due to their suitability to extruded the inks at the required flow rates.

All the components of the printhead were either opaque (the barrels) or were covered by an aluminum foil which served as a protective cover against reflected UV radiation, so as to ensure that only the dispensed ink is curing. A protective cover (**33**) was used to cover the tip of the extrusion needle from direct UV (**32**) illumination and prevent crosslinking of material at the tip.

During operation, one of the ink barrels was pressurized using the pneumatic system while the other two barrels were at atmospheric pressure. This forces the selected ink to flow while the check valves ensure that the other two channels are closed. The Priming volume or the dead space volume of the printhead after the check valves was about 130µl in the current configuration of which about 30µl is the internal volume of the needle holder and 100µl is the volume of the three to one junction and the associated connections. In the case of switching between the inks, this amount of volume of the previous ink must be extruded out before the new ink can be printed. However, since the volume is known precisely, it can be adjusted in the printing by looking ahead to the end of the printing of that ink and switching ahead of time so that the spatial pattern for the deposition of the ink is maintained and continuous printing can occur.

In other state of the art printer that operate with multi-material deposition, usually multiple tips are employed, each for a specific ink. Although, this is suitable for extruding thermoplastic materials, it is unsuitable for UV curing inks. When one nozzle is being used, the other nozzle tips with ink in them are stationary but exposed to scattered UV light. This will cause some degree of crosslinking in them leading eventually to needle clogging. In a single tip configuration, an ink flow is always maintained as long as light is shined upon the nozzle, which prevents tip clogging while enabling multi-material capability. In addition, continuous printing also eliminates the start and stop artifacts as well as alignment issues that may arise in multi tip printing.

4.2.2.Pneumatic system

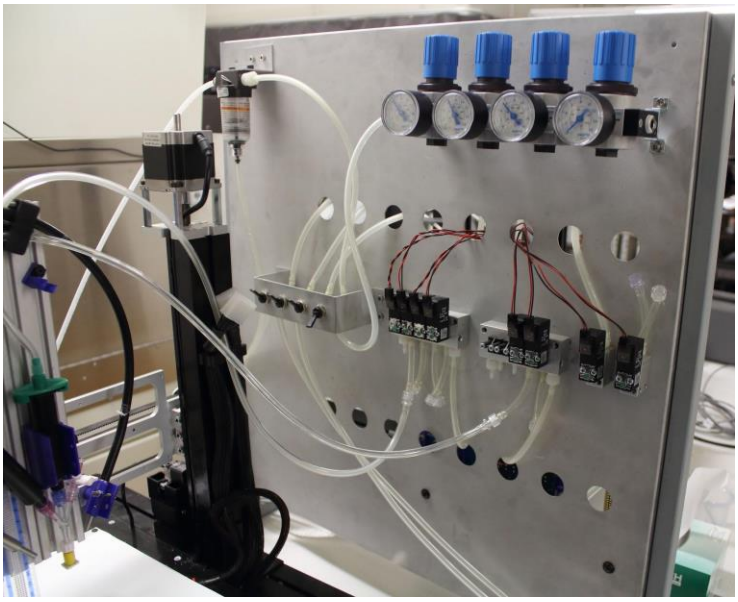

Figure 4.5, The pneumatic setup, in this configuration, ink A is connected to ch1 and ink B is connected to ch5, the pressure on both is set to ~90 Psi.

External pressure was provided by a 90 psi pressure supplier (**66**). The pressure supply was connected (**64**) through a filter to three control channels (**75**) each comprised of a regulator (**61**) and solenoid 3-way pneumatic valve (**62**), which can connect each ink barrel (**24,25,26**) either to a preselected pressure (by the regulator) or atmosphere. Each solenoid valve can be individually controlled by the control system (**75**).

The pressure to the system was provided by an external air pump (**66**), however, since the air pressure expenditure is minimal, a compressed tank can also be used. The pressure was used to actuate the printhead. The pressure control panel and all its components were fabricated and assembled for this research.

4.2.3.UV illumination system

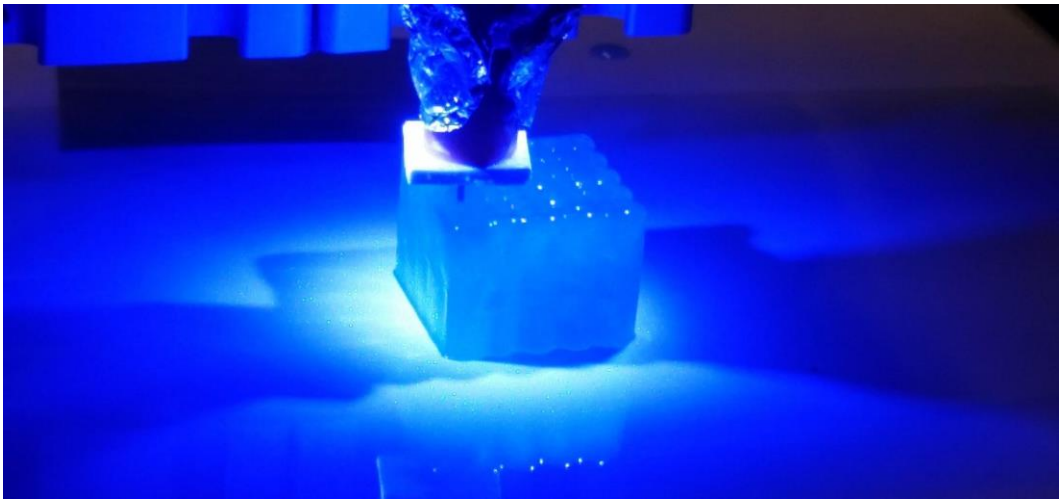

Figure 4.6, The UV light curing and illuminating the cube printing experiment, the silicone part is somewhat translucent, and so the light pattern is a combination of the direct illumination together with interesting reflection patterns. The shadow from the protective cover and its holder is visible on opposite sides of the cube.

The strong UV light required is provided by a UV curing system ‘Omnicure S1000’ (**54**) and routed to the printhead using two flexible light guides (**55**) which terminate on the sides of the printhead (**30,31**). the UV output was controlled in an on/off mode by the computer controller through one of the 12V channels (**75**). The S1000 curing system was able to provide 100W of UV power with most of the output in the 300nm-400nm range. the two light guide ends are fixed to the printhead at a distance of ~4 cm and angle of ~45° providing an average maximum illumination of $17.2W/cm^2$. Since the lightguides are fixed to the printhead, the UV spot is always focused on the tip of the nozzle and follows its movements. The direct powerful illumination ensures the fast cure that is required to stabilize the inks within seconds. The tip of the needle contains a protective cover that is located 5mm above the tip and has a 5 mm radius (see figure 4.7). This ensures that the tip is not exposed to direct UV light

4.2.4.UV exposure control

UV exposure control of the immediate area around the nozzle tip, as well as the point of deposition on the substrate, is critical for stable printing. Since the rate of the reaction is a direct function of the UV power and duration of exposure. It is desirable to ensure spatial control of exposure intensity to minimize curing where it’s detrimental and maximize where it’s useful. For this purpose, it is useful to identify spatial areas with reference to the extrusion nozzle in order to determine the light intensity requirements (See figure 4.7)

Sector I - The tip of the needle, a small (radius of ~3 mm) spherical volume just around the tip of the needle. This sector needs to be shadowed from the incident UV light as much as possible to prevent curing of the ink on the exterior of the needle.
Sector II - The area of direct illumination outside Sector I. This is the exposure area that rapidly cures the ink trace before it loses its shape. The stronger the illumination in this sector, the better it is for consistent trace dimensions (as shown in section 6.3). However, increasing the UV flux on this area tends to increase also the reflected portion affecting Sector I, increasing the associated problems.

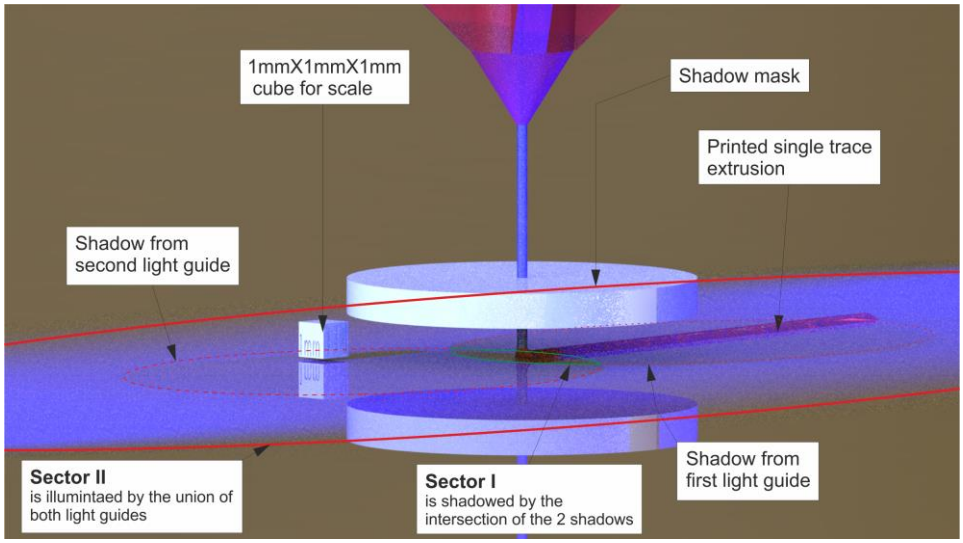

Figure 4.7, A CAD model image which illustrates the illumination sectors under the two light guides at 45 deg.

Sector III - The rest of the print area. Floodlighting for this area is beneficial to complete curing the traces after the initial printing. Since the total exposure from light in sector II depends on the printer’s movement, it might not be enough to completely cure all of the printed traces. Therefore, having a flood light which is independent of the printing head can be useful. However, it was not required in the work described in this thesis, as the illumination in sector II was sufficient to fix the trace.

To modulate the light levels in sectors I and II, as desired, a protective cover was added to the needle tip. The cover was fabricated of a round piece of PVC white plastic with a hole cut in its center, so it maintained its position on the needle with some friction.

4.2.5.Control system

The frontend control was provided by the ‘MachineFace’ networked GUI interface for machinekit developed by ‘The Cool Tool’™. Modifications to the GUI and the ‘Sandybox’™ config were incorporated to enable synchronous

control of the XYZ positioner, the solenoid valves and the UV lamp. The solenoid valves were controlled through a driver which was synchronized over a i2c communication bus. The communication between the control system and the solenoids is faster than 40 Hz, which is the mechanical response time of the solenoid valves.

4.2.6.Printhead operation

Once an ink barrel gets pressurized through its control channel, the pressure on the ink starts pushing it down into the junction, the pressure difference opens the check valve (there is a minimum opening pressure head of the check valve is below 5 psi) and enables the flow of that ink into the junction. The pressure rise in the junction then seals the two other check valves, preventing any backflow, and forces the ink to flow through the extrusion needle. The extruded ink is then deposited onto to the print surface.

The movement of the printer (XYZ) was synchronized with the valve control and the switch controlling the on/off state of the lamp through a central Gcode machine interface controller. A mechanical shutter controls the lamp on/off state and has a < 1 sec response time. Therefore, the sequence of inks flowing through the nozzle and its spatial deposition can be synchronized. Also, when it is required to stop the flow of the ink, it can be instantaneously stopped and simultaneously the UV light switched off so that there is no unwanted crosslinking at the tip.

4.3.Printer controller

As 3D printer technology evolved, specialized printer technologies have been developed for each 3D printing technology. If we look at the most common 3D printing method today for consumer use it would be the FDM method, of which the RepRap series is the common example. Common open source 3d printer use

technologies borrowed from decades of previous development for the CNC industry. And use many of the conventions and methods used by the CNC technology, such as cartesian machine coordinates, the use of a central interpreter and coding of the part into Gcode for the interpreter. RepRap also uses the Arduino stack for rapid development, this cuts down on cost and enables distributed development but comes at the cost of stunted capabilities and essentially a dedicated firmware for the FDM process.

Stronger system on chip development boards such as the Beaglebone, offer much superior extensibility to new 3D printing process development. Whole OS systems based on Linux such as the Beaglebone offer many advantages over the raw microprocessor boards such as Arduino. By enabling OS level file handling, concurrent processes, and support for high level languages. This is one of the main reasons for the use of the UNI-PRINT-3D [27] from ‘the cooltool’™, as it’s control board is a modified Beaglebone board. This allowed integration of the additional printhead control functions required as python programs.

5.Results

5.1.Actuation of the printhead

To determine the rheology and the flow rate response of the various inks through the printhead, a flow experiment was conducted. The flowrate(Q) of the custom inks (V35H, V31H and V21H) was measured in response to applied pressure through 22Ga and 25Ga diameter needles with ¼" length.

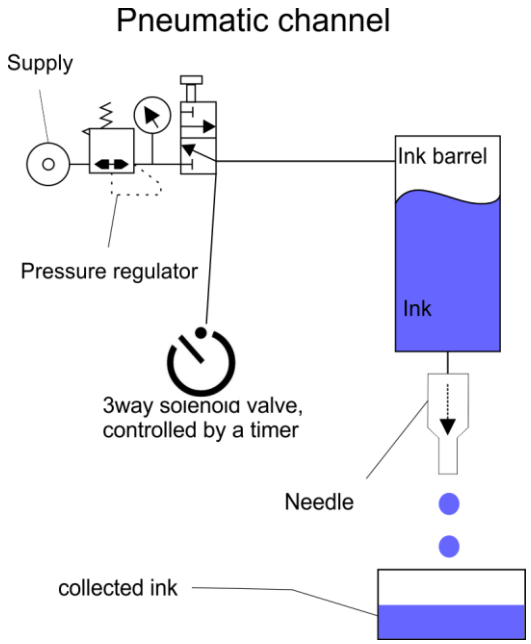

Figure 5.1, Single pneumatic channel setup for the flowrate as a function of pressure experiment

In this experiment, a pneumatic channel (Figure 5.1) with pressure control was assembled, using a typical pressure gauge (Festo, LRB-D-MINI,2 psi resolution - McMaster Carr). The pressure at the supernatant space of the ink barrel was switched between an on (pressurized) and off (depressurized) state by a solenoid valve that was controlled using a timer. Pressures from 10 psi to 90 psi was applied to the ink barrels containing the silicone inks using the pneumatic channel for predetermined duration of time and the amount of ink flowing through the nozzle (length of $13.2 \pm 0.1mm$) was collected and weighed to determine the

flow rate. Typical duration of time for pressurized flow ranging from 180s to 10s were used for the 22Ga ($430 \pm 5\mu m$) needle and 480s to 120s for the 25Ga ($280 \pm 10\mu m$), so that the net weight flowing through the nozzles were nearly the same. The experiment was repeated four times for every setting. A value of 0.96g/ml was used as the density of the ink (measurement made by collaborators).

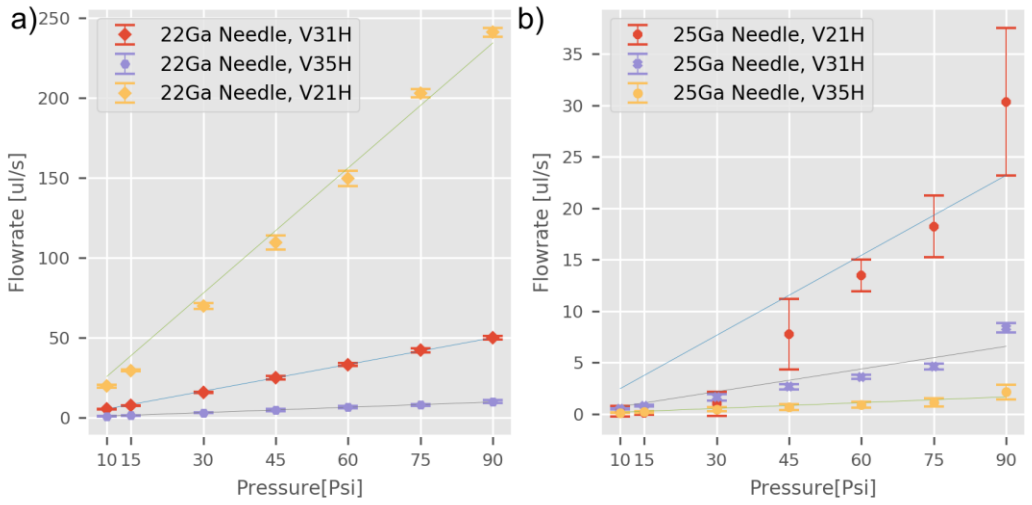

Figure 5.2, Flowrate as a function of Pressure, a) For 22Ga (413um) needle,
b) For 25Ga (260um) Needle. Included are the fits for the data, 1st order
The fitting data is provided in Appendix - Flow fits

The flowrate vs. pressure relation for these needles and inks is presented in Figure 5.2. The V31H ink and the V35H ink behave like a Newtonian fluid under the operating conditions as can be seen from their near linear trends, but V21H shows a more complex rheological character due to the presence of fumed silica particles in it (Table 3.2). Silicones with fumed silica additives are known to have thixotropic behavior. The silica particles absorb the silicone polymers onto their surface and create a network that leads to their thixotropic behavior. This behavior is evident in characteristics of the V21H ink through both the nozzles but is more prominent in its flow through 25Ga nozzle diameter. The thixotropic behavior is also the reason for the larger variability in the flow measurements for

the V21H ink. The adsorption and network formation over macroscopic scale can lead to instability in flow and could also lead to needle clogging over the long term. Indeed, V21H inks produced occasional clogging of the nozzle while other inks without fumed silica did not have any clogging.

A linear best fit was made to the data obtained for various inks and the slope was used to determine the viscosity using Hagen Poiseuille equation which are reported in the table below (Table 5.1).

Table 5.1, Ink viscosities calculated from the experimental data

Ink	**Viscosity[mPaS]**
V21H	168
V31H	787
V35H	3965

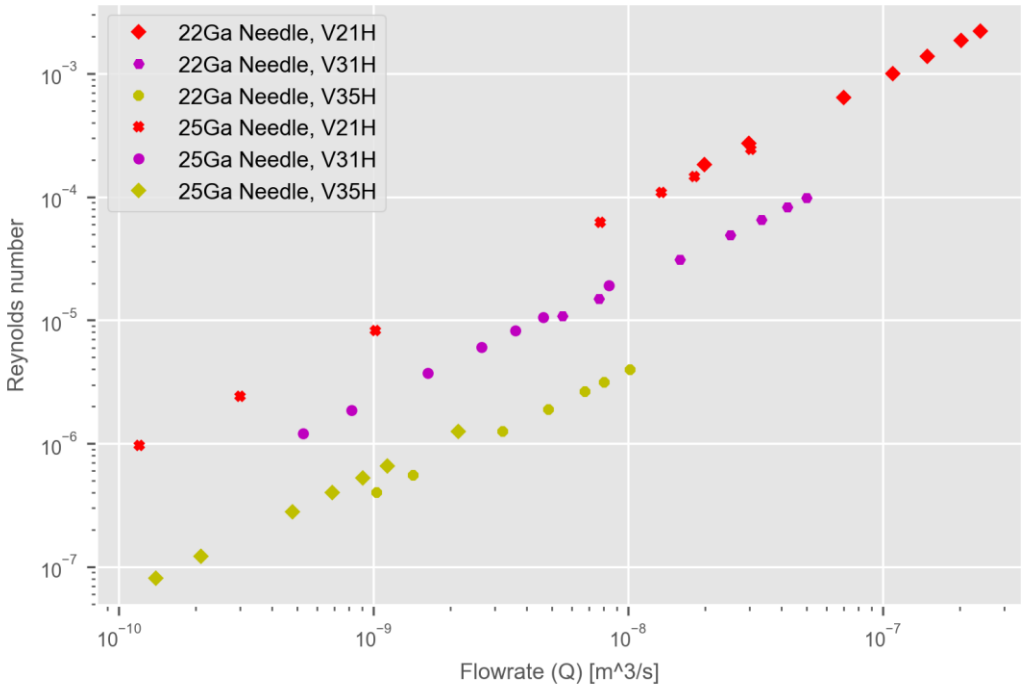

Figure 5.3, Reynolds number for the different ink and needles for the flowrate experiment

Figure 5.3, shows the Reynolds number calculated under various operating conditions and for the different inks used. The Reynolds number range is $10^{-7}$to 10^{-2}, and is clearly in the low Reynolds number regime where the inertial forces play no role in the flow dynamics. Viscous and capillary forces are more dominant as evidenced by the accumulation of the material extruded from the nozzle up its outer side to form a bulb of ink at the tip of the needle (figure 5.4).

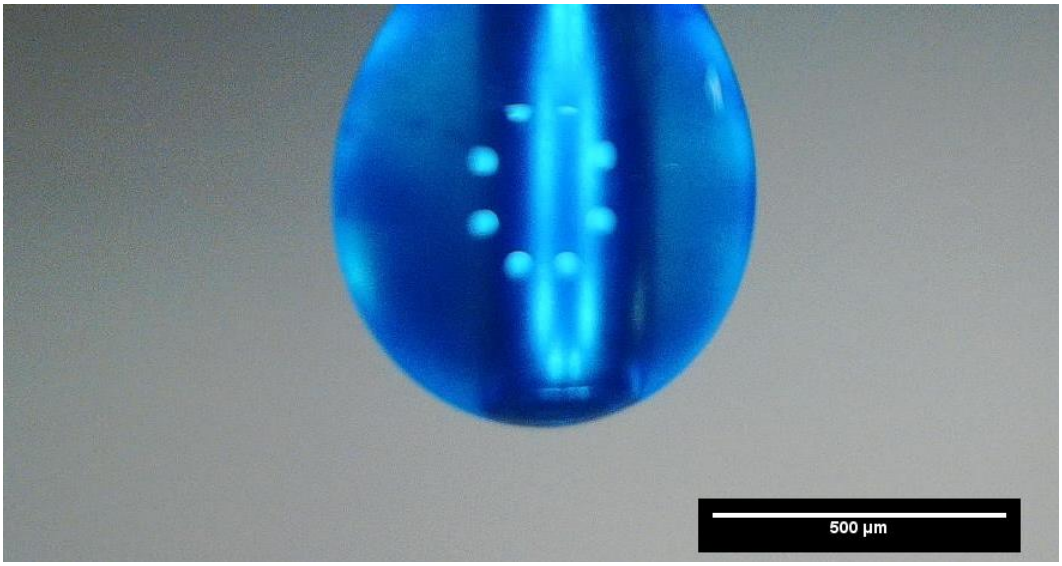

Figure 5.4, A microscope photo of V31H ink on 25Ga needle, forming a bulb covering the needle due to capillary forces pulling it up, even though the ink is still flowing through the needle, its inertia is dwarfed by the capillary forces forming the droplet.

Based on these experiments, thixotropic (V21H) inks containing fumed silica in them were found to be unsuitable for reliable extrusion and were not used further. Non-thixotropic inks (V31H and V35H) were found to be non-clogging and smooth flowing and were chosen for further use.

5.2.Effect of printing parameters on trace deposition

Initial experiments were conducted on thermally cured 'Sylgard 184' in order to determine the dynamics of the printing process and the critical parameters that determine optimal printing conditions. While being a different composition, it is similar rheologically to the UV inks that were used eventually, and thus valid observations can be made about its behavior which apply to the UV silicone inks as well.

Since the Sylgard ink comes in two parts a micromixer was used to mix the two parts before extrusion. Two syringe pumps were set up to pump both the curing agent (CA), dyed blue, and the base, dyed yellow, into a micromixer. The resulting mixed ink flows through a 22Ga needle and was deposited on a heated printbed. The printbed was set to a temperature of 110°C so that the deposited ink can be rapidly cured, fixing the trace shape following deposition. The mixing ratio of the CA to base used is 1:7 as the manufacturer recommended 1:10 does not mix enough for a homogenous material extrusion and retention of the printed shape.

The flow rate of the ink, the height of the nozzle tip from the substrate surface (Z offset) and the feedrate of the printhead where the parameters that were varied in order to characterize the printing process. In this experiment, two flowrates ($50\mu L/min$ and $100\mu L/min$ of the total ink flow), four Z_{offset} (0.1mm,0.2mm,0.3mm,0.4mm) and six feed rates (250,500,750,1000,1500,2000) [mm/min] were tested by printing a serpentine pattern of 20 mm length as shown in figure 5.5. These patterns were repeated four times for each combination of conditions. The ink was printed onto a glass substrate attached onto the printer hotbed with double sided tape. Following printing the slides were removed and imaged under a microscope with 4.5X magnification.

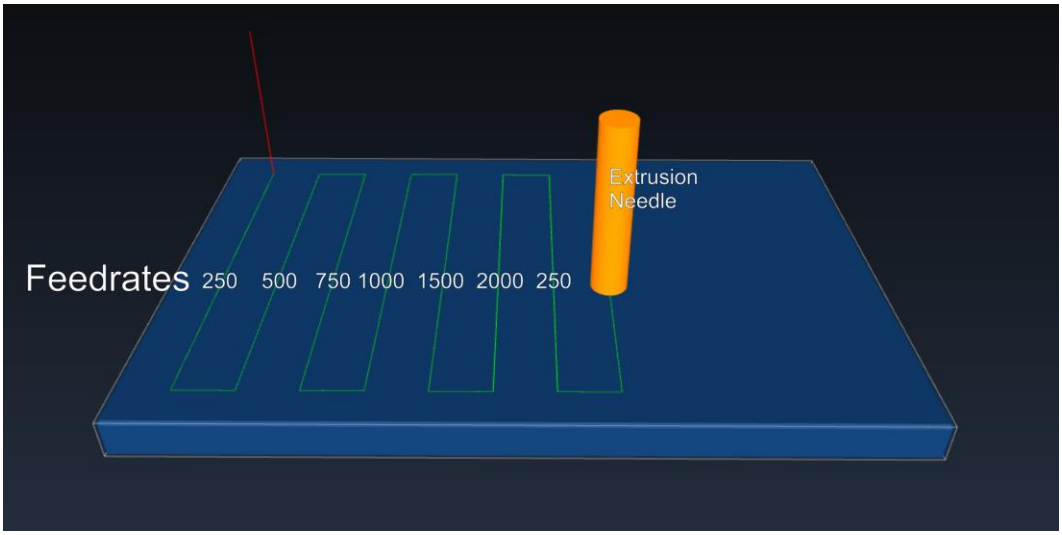

Figure 5.5, Shows a simulation of the print pattern with increasing feed rates left to right (and start of new set).

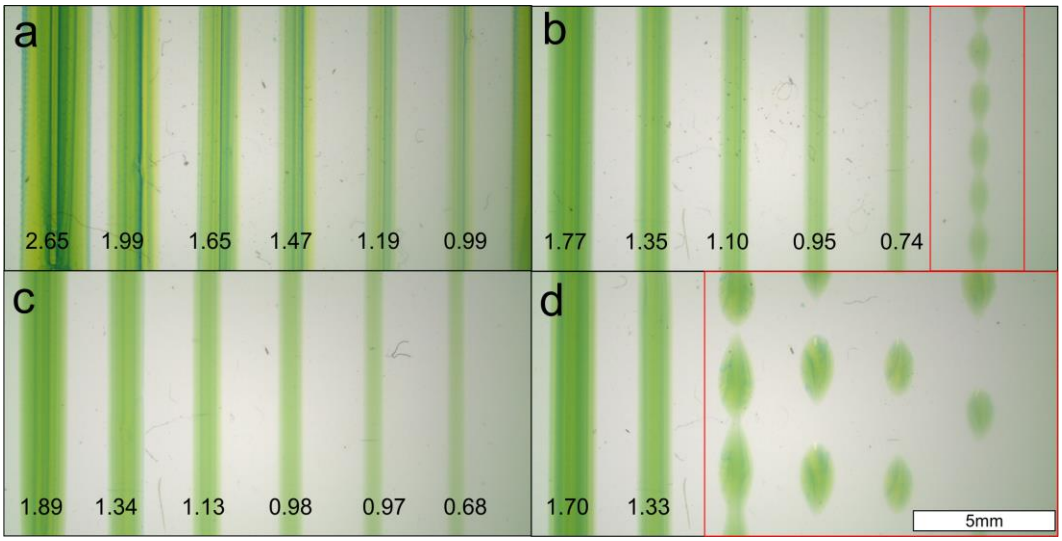

Figure 5.6, The resulting traces normal printing and periodic deposition in red. For normal prints the bottom number is trace width in μm

a)100µL/min,0.2Z_ob)50µL/min,0.2Z_o c)50µL/min,0.2Z_od)50µL/min,0.4Z_o

The printed lines are shown in figure 5.6 for various feedrates, flowrate conditions and offset spacing. It can be seen in figure 5.6a that the width of the trace reduces from $2.65 \pm 0.08mm$ to $0.99 \pm 0.06mm$ as the feedrate is increased from

$250\,\frac{mm}{min}$ to $2000\,\frac{mm}{min}$. Comparing figure 5.6b with figure 5.6a, it can be see that a higher Z offset also reduces the width of the trace. Similarly, comparing figure 5.6a with figure 5.6c shows that the reduction in flowrate can also reduce the width of the trace. This experiment demonstrated that extrusion of the silicone ink onto a substrate is possible and can produce continuous traces under certain feedrate and flow rate combinations. It was also observed that at low flow rate or at high feedrates or offsets the trace formed was not continuous and droplet deposition occurs. An example can be seen in figure 5.6d.

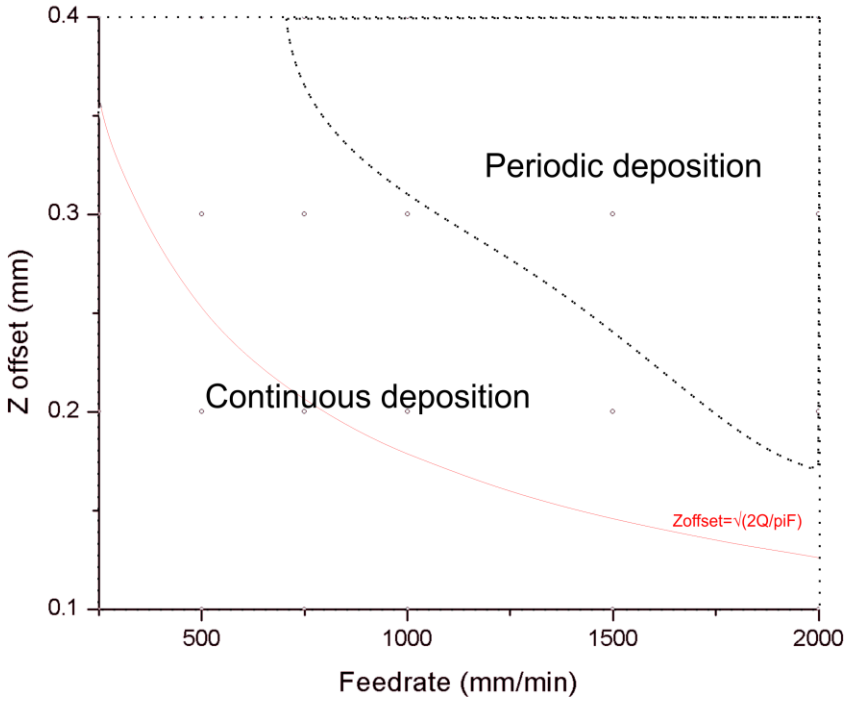

Figure 5.7, Shows the periodic and continuous deposition regions for the Q=$50\mu L/min$ condition. The red curve is the ideal condition theoretical result derived in section 5.4

The regions for feedrate and flowrate printing conditions which result in continuous or periodic deposition for a flowrate of $50\mu L/min$ are shown in figure

5.7. It can be seen that periodic deposition occurs above a certain ratio of Z offset to feedrate, as the Z offset is increased periodic deposition occurs at lower feedrates.

5.3.Imaging the periodic deposition transition

The continuous to droplet transition in the deposition is a very interesting phenomenon as it puts a limit on lowest resolution possible. In order to understand the origins of the discrete droplet generation under extrusion conditions an experiment was performed wherein the extrusion of the ink from the nozzle was imaged closely from the side. A handheld microscope[5] was fixed on the printhead using a specially designed mount, that allowed to focus on the tip of the deposition needle in real-time during the printing process. The printing was done on regular microscope slides with V31H ink and 30W UV power and a 25Ga needle as the extrusion nozzle. Two print settings, one continuous - [Z offset 0.6mm Feed 1000mm/m, Pressure 38 psi] and one discontinuous - [Z offset 0.6mm Feed 2000mm/m, Pressure 10 psi] were used to make videos on the process. The videos were then analyzed and stills extracted.

[5] Calestron™ 5MP handheld USB microscope purchased from Amazon™

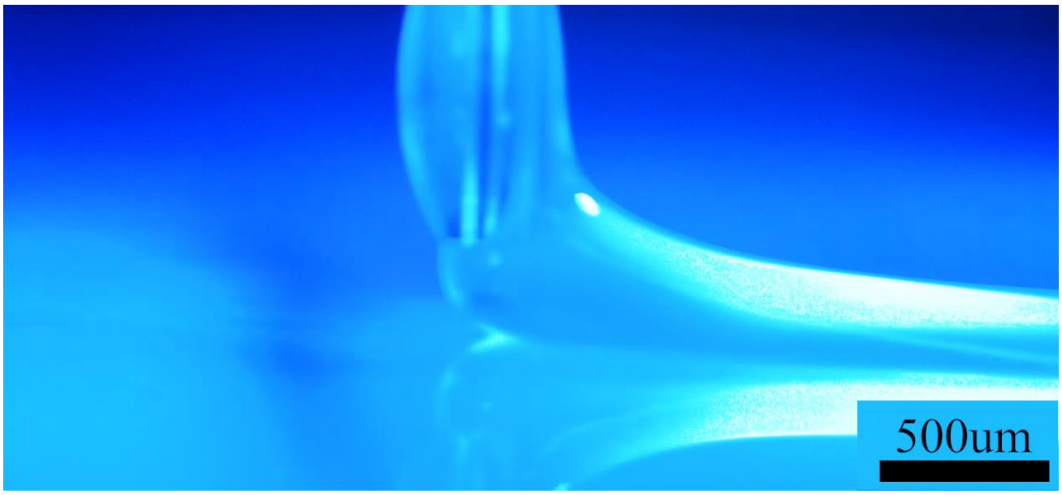

Figure 5.8, Image of the continuous deposition process.

Figure 5.8 shows details of the printing where the conditions produce a continuous printed line. It can be seen that the trace/flow is continuous and is not broken into droplets. The ink surrounds the nozzle as it emerges from it in the form of a drop which contacts the substrate underneath. As the nozzle moves, some of the ink is left behind which is then quickly polymerized upon UV illumination. It can be seen that the size of the drop around the nozzle rather than the nozzle dimension itself determines the size of the trace produced. Also, there is minimal slumping of the printed material as the UV intensity is high and the material is instantly polymerized. The height of the trace is determined by the gap between the nozzle and the substrate. The lack of pooling of the ink in front of the nozzle is indicative of the fact that the feed rate, flow rate and Z offset are well matched.

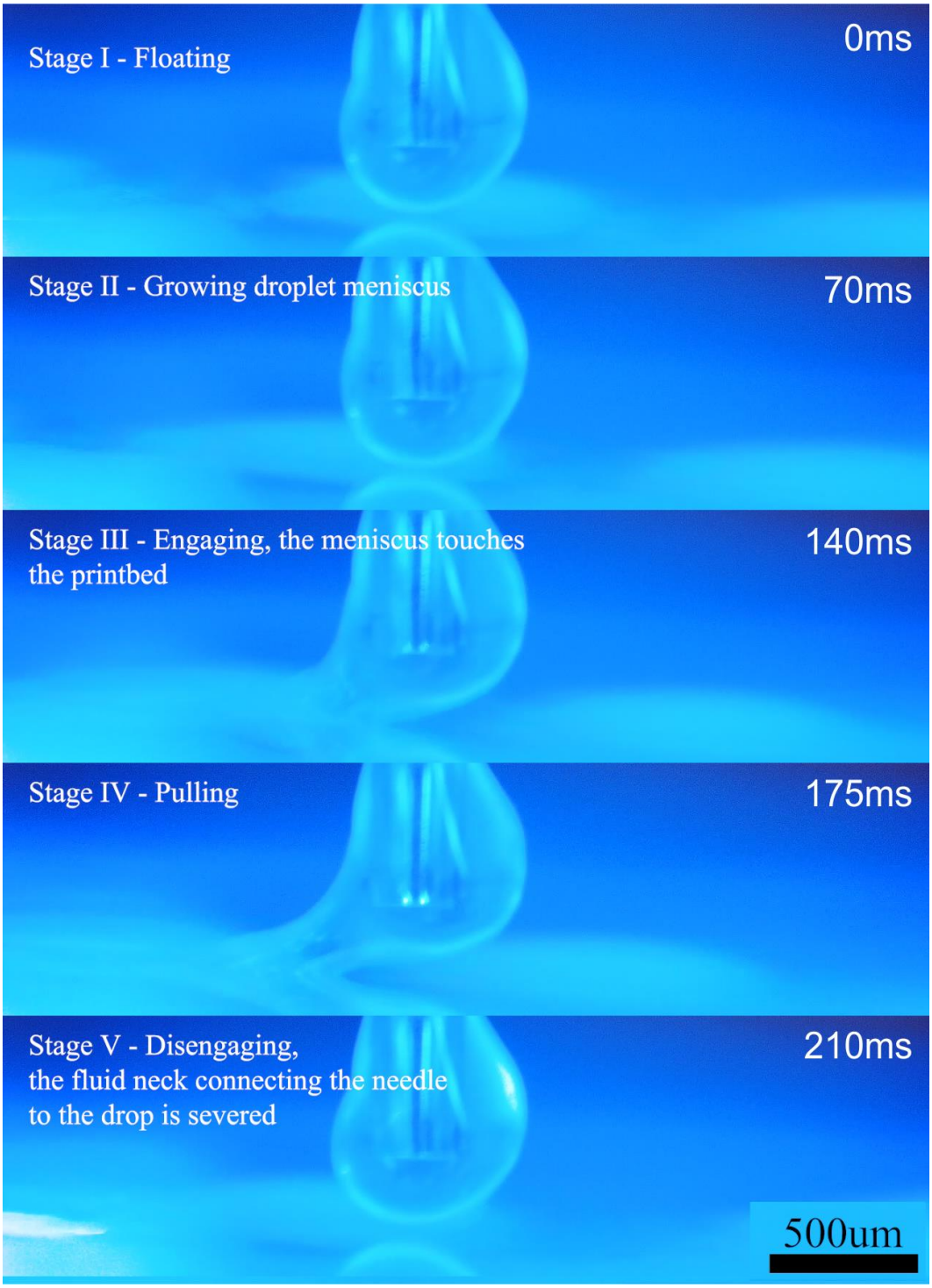

Figure 5.9, A composite from 5 stills showing the stages of the periodic deposition cycle. The large bulb of cured ink on the droplet is the undesired result of capillary flow of the ink up the needle followed by cure from indirect UV. Top right is the time sequence in milliseconds

On the other hand, when the feed rate, the flow rate and the Z offset are not well matched, then drop deposition occurs as shown in Figure 5.9. Initially, as the ink is pushed out of the nozzle, it accumulates on the outside surface of the nozzle due to capillary forces and forms a bead. At this stage, termed floating, there is no contact of the accumulating ink with the substrate and therefore there is no printing. The bead grows in size in the growing stage and it reaches a point where the accumulating bead comes in contact with the substrate. In this engaging stage, the ink wets the substrate and some portion of the ink is spread quickly on to the substrate which depletes the volume of ink on the nozzle tip. This causes the drop to be pulled up to the nozzle and the contact with the substrate is lost. A short line of material is printed on the substrate during the engaging stage. During the rest of the stages the droplet of ink is not in contact and there is no printing. These stages repeat cyclically producing an intermittent deposition of ink as seen in figure 5.6d.I. The bead of ink cured on the needle also grows in size in the process over time. It later either clogs the needle or dislodges into the print, ruining it.

This experiment shows that under suitable conditions (Q too low or Z offset too high), the continuous trace printing process can transition into a periodic deposition mode. In general, this condition occurs when the flow rate is not sufficient enough that a continuous stream can be maintained for a particular Z offset, feed rate and flow rate. In this case Z_o of 0.6mm, feedrate of $2000\,\frac{mm}{min}$, and pressure of 10psi.

The difference between a regular drop forming at an orifice tip and the above experiment, is because of two factors: The Z proximity of the printbed/print-layer to the lower lip of the extrusion needle is less than the height of the ink's drop that would develop had it not been there. The constant movement of said printhead during the printing process. Which means once an emerging drop is developing to a sufficient volume, it is engaged by the movement of the printbed or the previous

layer. In essence, the periodic deposition transition happens when the depositing process becomes unbalanced, and the system enters into a periodically dynamic mode, instead of the stable continuous deposition mode.

5.4.Theoretical model for deposition parameters

It is useful to derive a relationship between Q, F and Z_{offset}. A simple relation can be derived from simple mass conservation considerations. The ink volume being deposited can be approximated by a simple shape, such as a circle or a semicircle (Fig 5.10). The trace cross section area (A) is equal to the flowrate(Q) divided by feedrate (F) (Eq 7.1).

$$A = \frac{Q}{F} \tag{7.1}$$

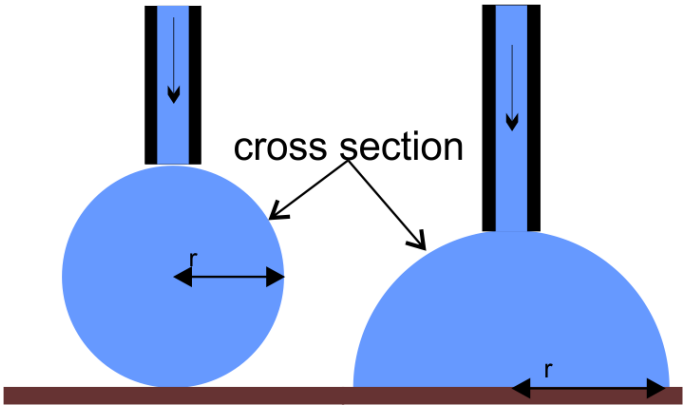

Figure 5.10, a model for the ink spread. The trace width can be considered as the radius of a circle or a semicircle

Since the area of the semi-circle is $A = \frac{\pi r^2}{2}$, equating the two yields:

$$\frac{\pi r^2}{2} = \frac{Q}{F} \tag{7.2}$$

With this geometric approximation $\boldsymbol{r}$ can be expressed as Eq 7.3 for a semi-circle or Eq 7.4 for a circle:

$$r = \sqrt{\frac{2Q}{\pi F}} \tag{7.3}$$

$$r = \sqrt{\frac{Q}{\pi F}} \tag{7.4}$$

The Z_{offset} required to stay engaged to the print can be the same as the r of the cross section derived from flowrate and feedrate. Since the ink is low viscosity and tends to flow after deposition, a semi-circle model for the appropriate distance can be used.

$$Z_o = \sqrt{\frac{2Q}{\pi F}} \tag{7.5}$$

This results in equation 7.5 which relates flowrate, feedrate and Z offset.

Plotting this relation over the printing results is shown in figure 5.7 in section 5.2. It can be seen that the Z offset suggested by equation 7.5 is safely below the periodic deposition region.

5.5.Characterization of the printed trace

A study of the cross-sectional shape of the printed trace was performed with an objective to determine the effect of various print parameters on the final trace shape. In order to ensure that the deposited traces are continuous, a design criteria of $Z_{offset} = 0.80\sqrt{\frac{Q}{F}}$ (as developed in section 5.4) was used.

In this experiment, a PVC transparent ¼" sheet was cut into rectangles of roughly 80mmx80mm to serve as a substrate, using the printer, a raster code was used to print two sets of traces of the V31H ink with varying feedrates on top of the PVC substrate, while the flow rate (and the pressure used to generate it) was held

constant. A single light guide was fixed at 4 cm and angle of CW 30° about X+ and about CW 20° about Z+. A power of 30% was used.
Various feed rates between 250 - 2000 mm/min and pressure setting between 30-90 psi was characterized. Two prints were made for each condition and each consisted of 10 repeated patterns. Also, traces were characterized when the nozzle was moving towards the light source and also away from it as the shadow of the nozzle creates a difference in the intensity of light impinging on the immediate vicinity of the deposited material.

The cross section of the printed trace is shown in figure 5.11. Each trace section was imaged and analyzed with the CV algorithm according to the trace sectioning method in Chapter 3. From the cross-sectional image, various parameters such as the trace width, height and area for each trace cross section can be extracted.

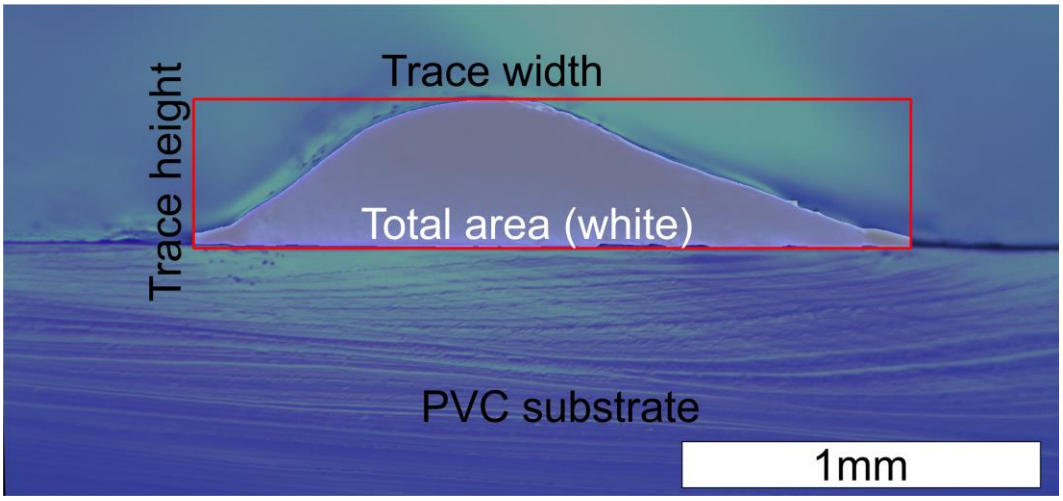

Figure 5.11, An example of a processed trace cross section image, printing conditions P-75 Psi, Feed-500mm/min, fully illuminated

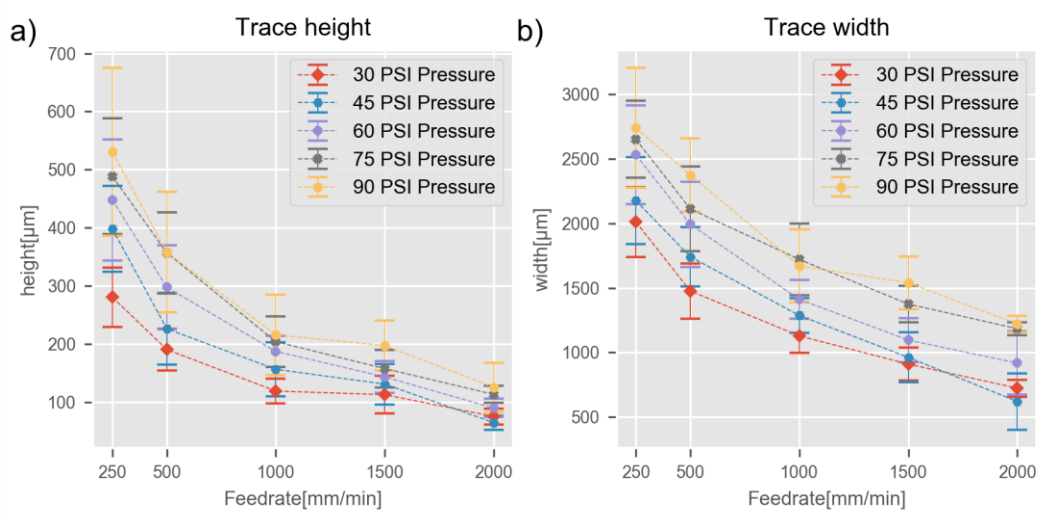

Figure 5.12, Trace height and trace width as functions of P and F, each point represents four samples, V31H ink

The trends in the trace height (fig 5.12.a) and the width (fig 5.12.b) as the feedrate was changed are displayed in figure 5.12. It shows that the height of the trace and its width reduce as the feedrate is increased. It also shows that as the pressure (or the resultant flow rate) is increased, the width and the height of the trace also increases. Nevertheless, the variation in each combination of pressure and feedrate seems to be quite large.

However, if the data was further categorized by travel direction as in figure 5.13, which affects the amount of illumination that is received by the material deposited, a bimodal distribution of the width and the height can be observed.

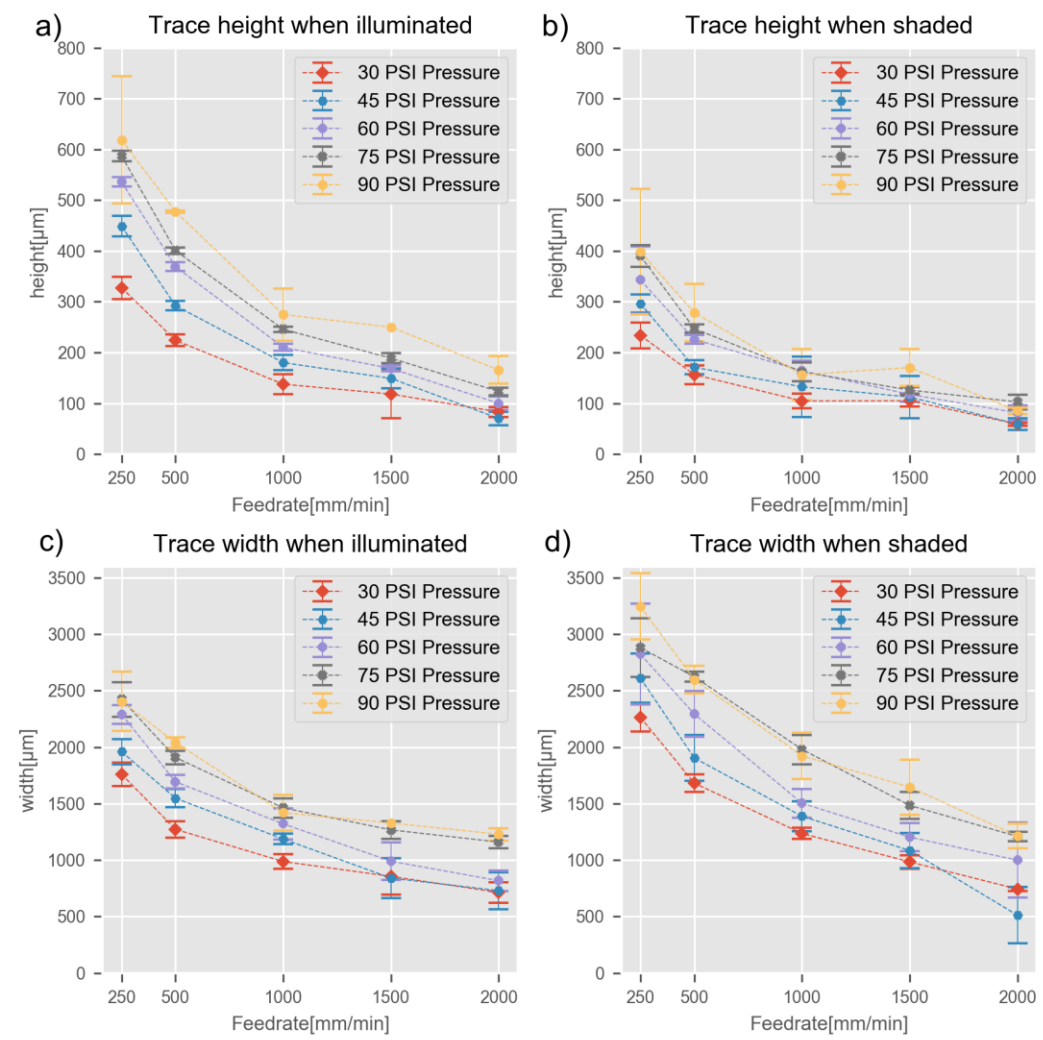

Figure 5.13, Trace height and trace width as functions of pressure, feedrate and illumination state- shaded/illuminated

The significant difference between the two directions illustrate that the short timeframe (sub second) following deposition is critical as it has a very strong effect on the resulting trace shape. This can be seen by comparing the absolute width (fig 5.13.c,d) and heights (fig 5.13.a,b) for the same conditions but different illumination.

For example, for 60 psi pressure and feedrate of 250 the illuminated trace is about $550\mu m$in height while the shaded one is $350\mu m$.

The bimodal distribution is better illustrated when the aspect ratio (height/width) of the trace is plotted against the feedrate as shown in figure 5.14

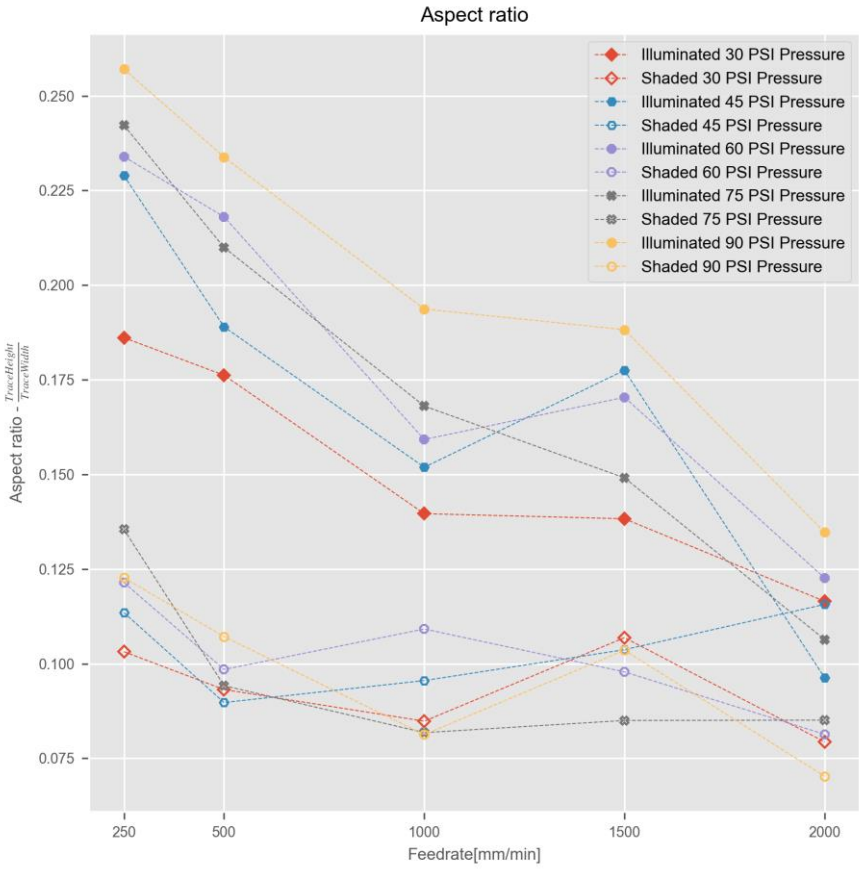

Figure 5.14, trace aspect ratio as a function of feedrate

It becomes clear the illumination state has a very important effect on the trace shape, with the shaded traces being much flatter and wider than the illuminated ones. For the shaded traces, the AR is reduced initially, however following that, the change is minimal for subsequent feeds.

While the illuminated traces AR is clearly inversely related to feedrate. This is an interesting result as one would not expect the AR affected by trace scale.

The experiment showed that the UV illumination plays a critical role in the final shape of the trace, and shadow zones need to be avoided. This conclusion was incorporated into the printer design by adding a second lightguide opposite to the first, creating a fully symmetrical illumination pattern.

6.Object printing

The previous chapters have dealt with different aspects of the printer, the deposition process and its properties. 3D printing however requires successful deposition and integration of multiple layers of material in a controlled manner over prolonged printing times. This chapter presents a few experiments on printing of 3D objects demonstrating the capabilities of the developed process.

6.1.3D cylinder

To show successful stacking of multiple silicone layers into a single object and to demonstrate that the combination of low viscosity silicone coupled to a rapid curing reaction can create a high aspect ratio 3D object without slumping or reflowing, an experiment to print a tall 3D cylinder was done.

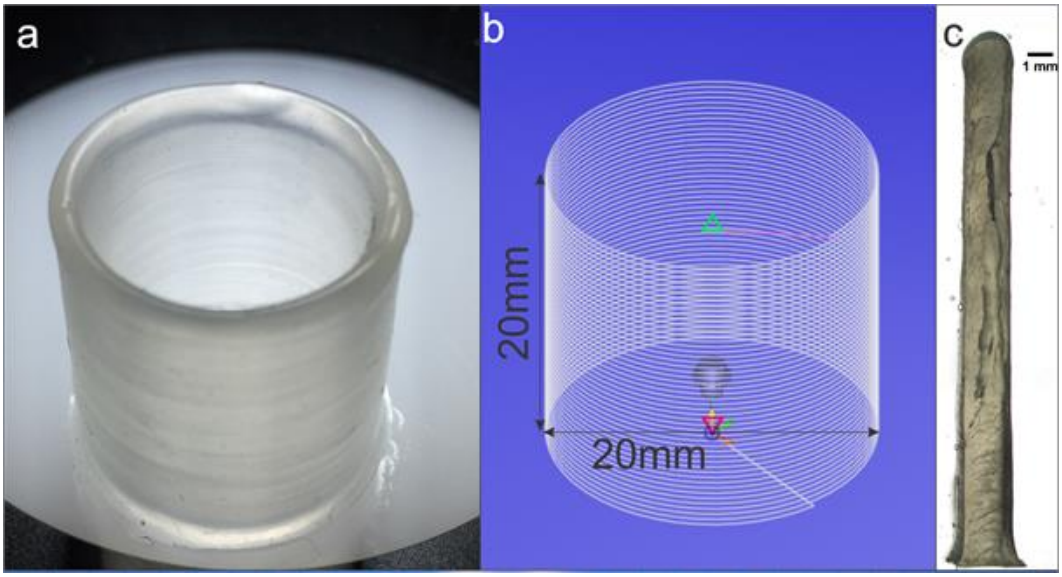

Figure 6.1, A 50-layer Silicone cylinder 3D printed using V21H ink. a) The cylinder b) A toolpath for the cylinder with dimension c) Z cross section of the cylinder.

The toolpath for the cylinder was coded manually and is a 50-layer single helix with a diameter of 20mm and a height of 20mm (see figure 6.1.b). The ink that

was used was V21H deposited with the 22Ga needle under a pressure of 24 kPa (3.5psi) producing a flow rate of 12.7 ml s^{-1}, the UV power used was 30% of the maximum(30W) or $5.1W/cm^2$. Using a feedrate of 1000mm/min each layer took 3.7 seconds resulting in total print time of 3.15min. After successful printing the cylinder was carefully cut along the Z direction and imaged with a microscope to examine its cross section and conformity (Figure 6.1.c).

The printed cylinder measured 20.9 mm in diameter 20.8 mm in height, the cross-section thickness was measured at 1.9 ± 0.1mm, with a small flaring on the lowest layer of 2.7mm, probably as a result of the difference in surface tension forces between the substrate and the subsequent silicone layers.
The printed cylinder had no discontinuities or voids, this is due to the unique property of the low viscosity ink to reflow slightly after deposition and then fix in place. The layers were well integrated with each other that the cross-section uniform walls do not reveal the boundaries between the individual layers.
The cylinder exhibited normal elastomeric properties and could bend and deform upon application of manual force, returning to its printed shape immediately after. The cylinder cross section is thus 10:1, taller structures are possible but the printing was capped at 20 mm due to the cylinder entering into a resonance with the printer's motors, making further deposition impossible. This is however a property of this specific structure, and not the process.

This demonstration successfully showed that it is possible to create high aspect ratio 3D objects using the UV silicone inks with the built printing system, it showed the low viscosity ink's tendency to conform to previous layers producing very smooth features. It showed that 3.7 seconds was enough time for a layer to cure well enough to support the stacking of the next layer, proving that the rapid curing of low viscosity ink is a viable printing strategy.

6.2.Discrete features

To demonstrate the possibility of printing discrete disconnected 3D structures a 'McMaster' sign was printed, (see figure 6.2)

Figure 6.2, a) 3D Printed V31H 'McMaster sign. b) The toolpath for the above sign green path is regular moves, red moves are rapid moves.

Printing techniques which employ constant displacement such as syringe pumps do not allow rapid interrupting and resuming of the ink flow due to the hydraulic capacitance, however using pressure control, rapid pressurization allows having fast switching of the ink flow on and off. The sign in figure 6.2 is a demonstration of this ability. It is composed of 30 layers of 0.15mm spacing, made of V31H ink with blue pigment. Extruded with the 25Ga needle with a (620 KPa) 90 psi pressure resulting in 9 µl s^{-1} flowrate. The printed toolpath was 16.4m long with 307 rapid moves and it took 18 minutes to print. The printed sign size was 136mm(X)x54mm(Y)x4.7mm(Z). by switching the pressure off in the rapid moves using the pressure control synchronization of the printer, each letter is printed separately from its neighbor and the rapid moves between and inside the letters leave little to no ink. Even though each letter is distinct there is slight bulging in some of the points where the printed head is decelerated or when a rapid move crosses over an already printed trace. The bulging in the first case is due to some residual pressure results in a small drop of ink to grow as the needle

disengages from a trace, this drop then gets deposited in the beginning of a new trace. Or in the second case, gets deposited onto an existing trace as the needle passes over it. Those effects however are minimal and do not interfere with the print resolution.

The 3D 'McMaster' sign demonstrated the capability to print discrete features, this especially important in application to more complicated prints, where each layer is composed of many regular traces bridged by jumping rapid moves.

6.3.Hollow hemisphere

A challenging feature for any 3D printing technology is overhang printing. And doubly so for low viscosity inks which if left uncured would flow down in matter of seconds. However, the combination of the low viscosity inks with the rapidly curing UV thiol-ene chemistry allows to print even some overhanging structures. To test whether the ink's curing rate was enough to support overhangs. A freestanding hollow hemisphere was 3D printed without the use of any overhang support.

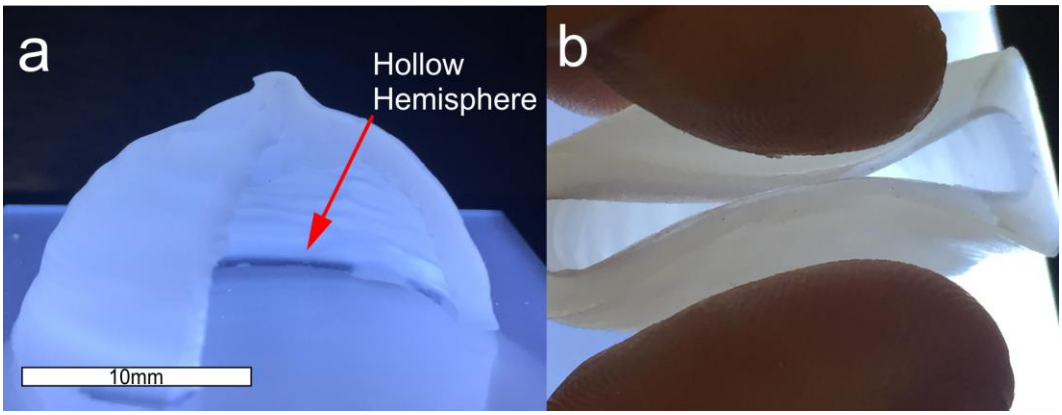

Figure 6.3, a) A hollow hemisphere printed using V21H with a cut introduced for better view of the internal section, b) The hemisphere under stress showing the flexibility of the printed elastomer structure.

The hemisphere in figure 6.3 was printed using V21H ink with the same parameters as the cylinder in figure 6.1 (24 kPa (3.5 psi), 12.7 ml s^{-1}).
The sphere diameter is 30mm and the print took 220s at a feedrate of 1000mm/m. The wall thickness was measured at 2mm. There is slight drooping when the overhang reaches 70°. However, the ink still cured rapidly enough to support the following layers.

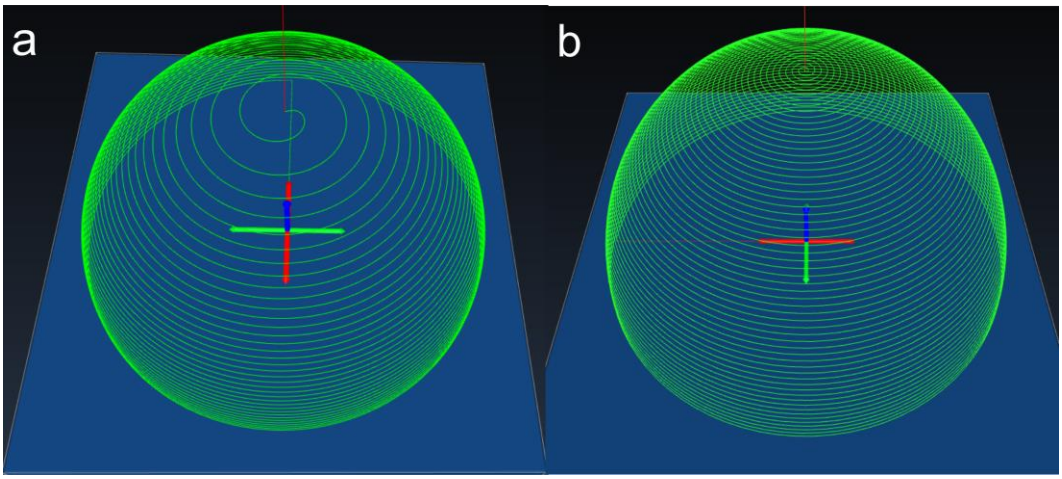

Figure 6.4, The overhanging sphere toolpaths a) Rastering by Z height b) Rastering by θ angle.

The toolpath was generated manually and two toolpath generation techniques, as shown in figure 6.4, were tested, typically most 3D prints are sliced by Z height, where each layer is of constant height. This was the first strategy attempted. However, this approach failed because the lateral layer to layer distance increases gradually as the print approaches the top of the printed structure. When the layer to layer lateral distance is larger than the width of the printed line, the printed line can no longer be supported and falls down. Therefore, the toolpath strategy was revised and the toolpath was instead generated with incrementally increasing θ angle (in spherical coordinate system with the middle of the hemisphere as its origin) of 1.5° increments, which at this diameter corresponds to vertical distance of 0.4mm. Using this method each trace is the same lateral distance and not only

Z distance from the previous trace. By using this method the printing proved successful.

This experiment demonstrates that the low viscosity ink fluid behavior was more than compensated by the rapid UV curing, allowing fabrication of free standing overhanging features, provided the tool path used maintains adequate trace to trace proximity conditions.

6.4.Solid cube

A solid 3D cube has been printed to show stable printing over a long period and the ability to create a single fused object of centimeter dimensions.

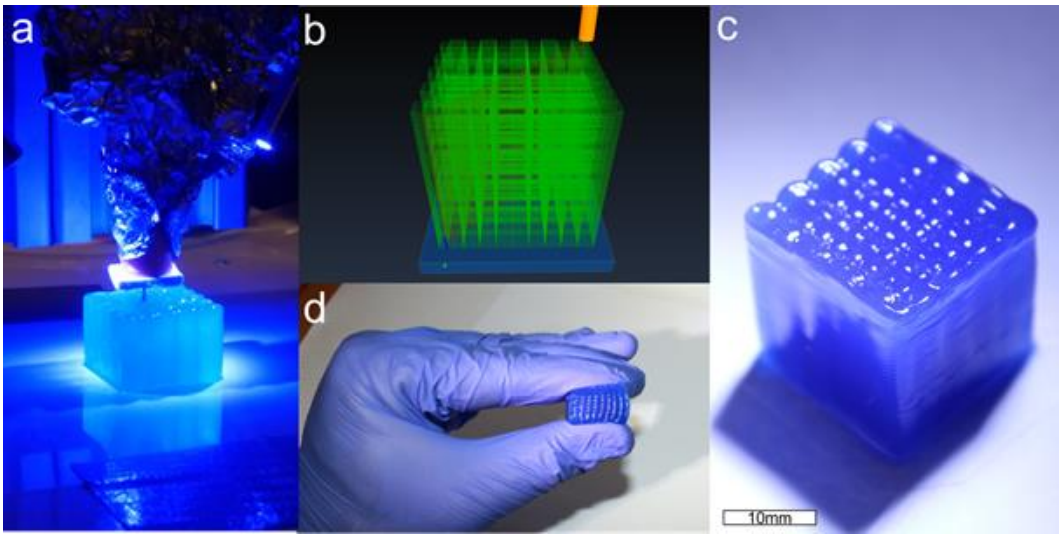

Figure 6.5, a) The cube during printing, showing the illumination pattern and the ink deposition process. b) The toolpath used to print the cube c) The printed cube d) A demonstration of the cube's elasticity.

The cube was printed utilizing V31h ink at 90psi using the 25Ga needle, corresponding to $9\mu l/s$ flow. The UV intensity was set at 30% (30W). And the feedrate was set to 1000 mm/min. The cube toolpath design dimensions are 19mm(X)x19mm(Y)x19.8mm(Z) with a trace to trace distance of 2mm and layer

to layer height of 0.3mm. The layer height was selected in accordance with the established results in Experiments. Graph 5.11. Each layer was composed of 10 lines in the X direction and 10 in the Y direction that forms a checkerboard pattern. And the cube is composed of 66 layers in total.

The printed cube dimensions were measured at 19.6mm(X) x19.1mm(Y) x19.8mm(Z). With the cube’s top surface clearly showing the 2mm XY raster pattern (Figure 6.6.b). The cube’s bottom surface (Figure 6.6.c) includes small voids between the overlapping traces, this is due to the less than 100% fill ratio. It also shows that the interface between the X and Y traces is invisible, and the ink traces merge into each other.

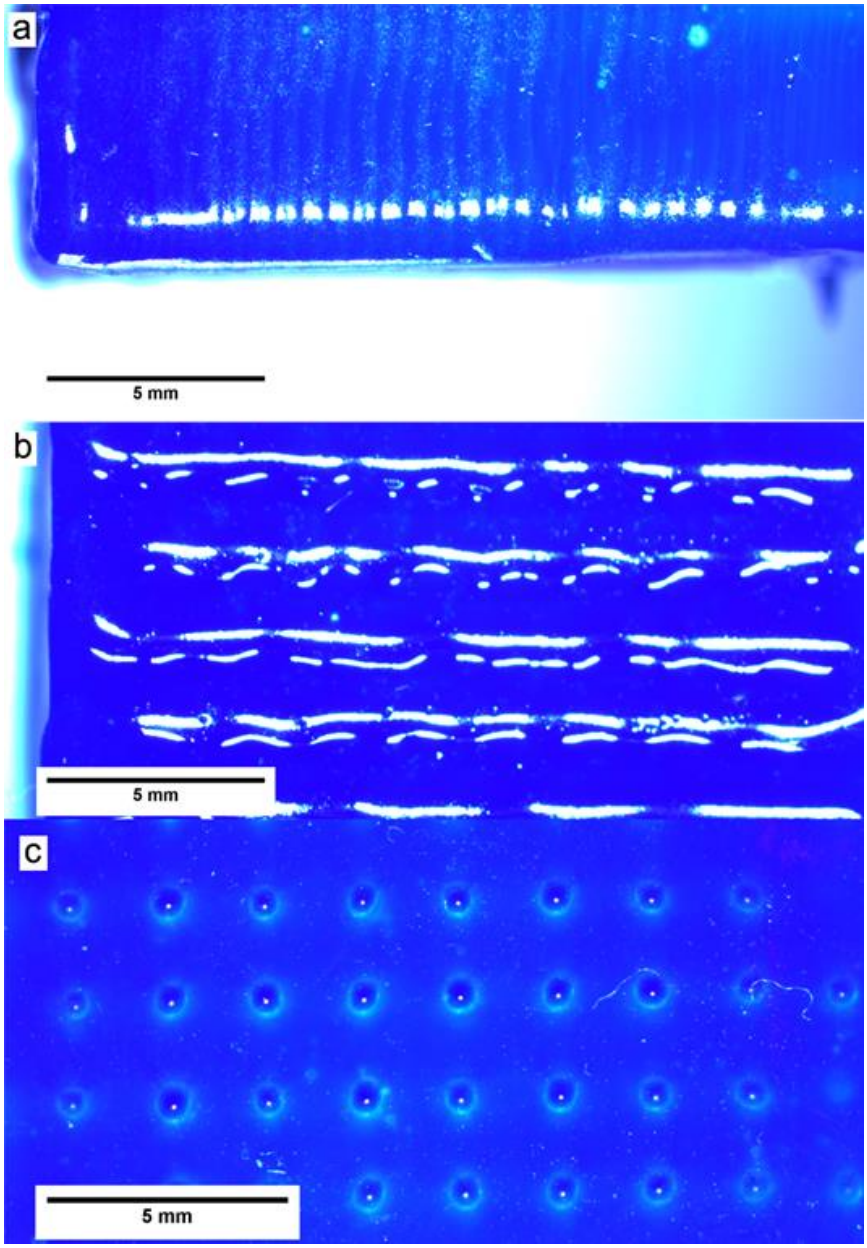

Figure 6.6, a) The Y-face of the cube, shows the layer stacking on the cube under microscope. b) The top surface of the cube, shows the valleys and hills terrain resulting from the raster. process. c) The bottom surface of the cube, the infill voids are the small inverted bubbles with 2mm periodicity (the path spacing).

The cube’s side surface (Figure 6.6.a) shows the smooth transition between the layers, demonstrating the ink’s conformal nature. The total print time was 38min. Excluding cleaning the needle’s exterior once without stopping the print, the printing was stable and continuous, throughout the entire time.

This print showed that whole objects with significant print time can be 3D printed, with the deposition process staying stable throughout the process. The final object dimension closely matches the designated shape. The trace height experiment proved useful in determining correct overall layer height according to selected deposition parameters. And the ink’s low viscosity is crucial for the smooth walls of the final object.

6.5.Multi-ink printing

The main objective guiding the design of the printer structure and the topic of the research is to enable multi-ink printing and fabrication of a single object with different constituent materials at selected parts of the object. This capability is demonstrated in two prints showing two different modes of ink switching.

The printhead merges the flow from three ink reservoirs into one extrusion channel which then connects to the deposition needle. The volume of the merging junction and in the line between the junction and the needle tip represents the priming volume of the printhead. To switch inks, this volume needs to be cleared of the previous ink to allow the new ink to reach the deposition tip. Thus, the two envisioned modes of ink switching are: purging ink switching and continuous ink switching.

6.5.1.Purging ink switching

In purging ink switching, to switch ink, the printhead first disengages the print, the UV light is turned off, the pressure to the active ink is removed, the printhead traveled to a predetermined purge location and pressure to the new ink is activated. This purges the old ink and primes the priming volume with the new ink. Since the volume of that priming section is fixed, the length of time the purging operation takes varies inversely to the flowrate.

One experiment to demonstrate multi-ink printing with two inks, employing the purging switching method was done by printing a ‘cake’ with five sections, two sections of V31H ink and three sections of V35H ink, each such section is made of 10 individual layers (see figure 6.7).

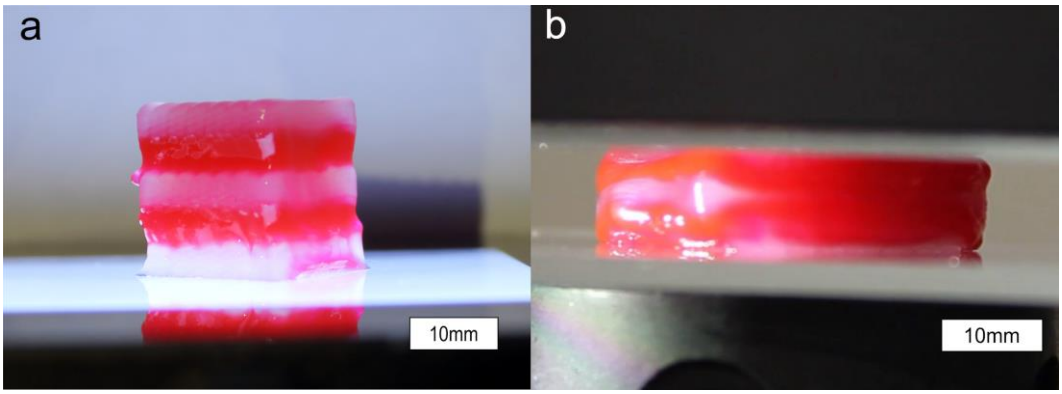

Figure 6.7, a) The full five section ‘cake’, white layers are made from V31H, and red of V35H. b) The ‘cake’ under 50N compression, with the softer V35H ink bulging out.

The toolpath dimensions of the cake are 15mm(X)x15mm(Y)x15mm(Z). The deposition conditions used here were the same as those use in section 6.4 for the solid cube printing. To compensate for the lower flow rate of V31H at the operating pressure of 90 psi, the feedrate used was 500mm/min compared with the 1000mm/min used for the V31H ink. Both inks used 0.3 as the layer height and 2mm trace to trace spacing.

The total printing time was 16 min, of which 4m10s was used for the five ink switch procedures. The ink switching happened successfully. And the border between the two inks is clearly defined (see figure 6.7.a). The two inks have different optical as well as mechanical properties, with V35H being softer than V31H, this as well as the object’s overall elasticity was shown in a compression demonstration, where the cake was subjected to 50N vertical compression (see figure 6.7.b). The deposition rate between the two inks was not perfectly matched resulting in slight bulging of the red V35H sections (figure 6.7.a). However, this can be overcome with more precise operating conditions selection.

This printing experiment has illustrated the ability to 3D print a complete object with multiple separate regions of different mechanical and optical properties. The separate regions adhere well to each other and the resulting object is solid without visible delamination. The purging ink switch method is most suited where the number of ink switches is limited as each switch requires lengthy purging period (50s in this experiment) and a volume of ink equal to the priming volume must be discarded in each switch.

6.5.2.Continuous ink switching

In continuous ink switching, the printhead does not disengage the printed object. Instead the pressure is switched instantly from the old ink channel to the new. This enables a faster operation but results in a lag between the ink switch command and the actual switch at the needle tip. The resulting transition between the two inks is also more gradual. If the switching rate is faster than the lag, the ink slugs form a first-in-first-out stack in the priming section.

This approach is shown in the printing of one cylinder composed of three cyclically alternating inks (Figure 6.9)

.

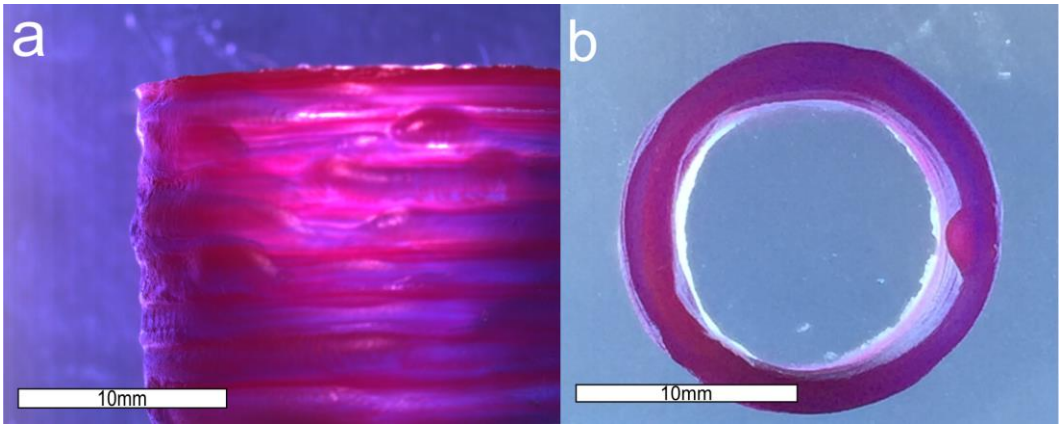

Figure 6.9, A side (a) and top view (b) of the three-ink cylinder print

The cylinder in Figure 6.9 is composed of three colored inks: clear-V21H, blue-V31H, red-V35H. The ink used changes cyclically every two layers for a total of 54 layers. Each layer is a height of 0.3mm. The toolpath diameter is 20mm and the height is 16.2mm. The pressure used for all three inks is 30psi. and the nozzle used was 25Ga

The print shows the periodic pattern of changing inks; however, the change is gradual, and all three inks traces form a trace coiling into the cylinder.
The printing parameters are not compensated for each ink’s flow response, and this results in the V21H clear traces being wider than the V31H blue traces, with the V35H red traces being the thinnest. However due to the low viscosity properties of the ink, the more fluid V21H is able to fill the height gaps left by the other smaller traces. This results in slight bulging to the sides as seen in the top of figure 6.9.a.

This result proves that the inks can be switched in a continuous manner and get deposited in a stacked fashion. The different inks form a single object with

gradually varying properties. A better control and timing scheme is required to compensate for the inks different viscosities in real time during deposition to ensure consistent trace dimensions. However, the V21H ink’s fluid behavior has a measure of compensation by flowing and filling whatever space or void left by the lower traces.

7.Conclusion and future work

7.1.Conclusions

In the course of this research a novel 3D printer has been designed and implemented. A commercial 3D printer has been modified with both hardware and software to control the actuation of a printhead which supports the printing of three UV curable silicone inks of different properties. For this purpose, inks based on thiol-ene chemistry have been formulated by our collaborators and shown to cure in a sub second time frame under UV light.

The flowrate to pressure response have been characterized. The parameters affecting deposition have been investigated, and the two modes of deposition. A theoretical model to keep the printing in continuous mode is proposed. The trace height, width and shape for one selected ink have been characterized.

Integrating these results enabled the 3D printing of complete objects. Printing of the 3D cylinder showed that the deposited traces solidify enough to support stacking and the creation of a high aspect ratio (10:1) structure. Printing of the ‘McMaster’ sign showed printing of discrete features with rapid actuation, without excessive dripping. Printing of the hollow hemisphere showed the printing of overhanging features. The solid cube printing has demonstrated the stability of the printing process over a period of 30 min.
Two switching modes have been demonstrated in the multi-ink printing experiments. A purging ink switch provides distinct material domains and a simple control scheme, while non-stop ink switching offers non-stop printing with multiple inks, conserving ink and time but requires a more complicated control scheme. Both schemes were used to produce 3D objects.

7.1.1.Balancing of printing parameters

Early experiments outlined in section 5.2 have shown that the selected ink’s low viscosity coupled with the rapid curing rate, require a balancing of the operating conditions, mainly the flowrate, feedrate and Z offset. This is required to keep the deposition process in stable and continuous deposition mode. If the deposition becomes unbalanced it may switch to a periodic deposition mode, which produces discrete drops instead of a continuous trace. The periodic deposition process has been imaged up close in section 5.3. A simple relationship developed from mass conservation was developed to relate the flowrate, feedrate and Z offset. Utilizing this relationship in the next deposition experiment in section 5.3 has proven successful by producing traces as small as 600µm width and 80µm height without switching to periodic deposition.

7.1.2.Importance of UV exposure control

Controlling the areas of the deposition process exposed to UV illumination has been found to be quite important. Early experiments without the integration of the UV protective cover presented many clogging issues, due to ink curing prematurely while still in direct contact with the exterior of the needle. Integration of the protective cover slowed this process enough to enable continuous deposition for the 3d printing of complete objects such as solid cube printing in section 6.4.

7.1.3.Printhead actuation

The choice of a pressure drive over a syringe pump drive was proven advantageous. By designing and integrating the custom pressure control system presented here, advanced printing features become possible.

Before application however, a pressure flow control scheme required calibration of the pressure to flowrate response. This was the purpose of the experiment in 5.1, by measuring the response of the three inks it was possible to determine the range of pressures suitable for printing for each ink.

Discrete feature printing was demonstrated by the ‘McMaster’ sign experiment in 6.2, this print has many rapid moves without excessive dripping made possible by the pressure control actuation rapid response. By externalizing the pressure control elements to the external control board and only routing the pressure lines to the print head, the printhead is made compact, enabling the incorporation of multiple inks on the printhead, in the current setup three inks are used, however, the printhead design allows for many more inks, making the printer design suitable for adaptation to other multi-ink applications such as bio-printing which requires a multitude of bio-inks. Finally, the pressure control enables simple ink switching as demonstrated by the experiments in 6.5.

7.1.4.Rapid curing of low viscosity inks

Low viscosity silicone presents some unique challenges to direct-write 3D printing. In other research, the methods employed include using of high viscosity silicone [3][7] or constraining the printing process in a support medium [4][5]. However, the UV thiol-ene chemistry inks combined the strong 100W UV illumination offered by an external UV curing lamp curing demonstrates that low viscosity silicone inks can be successfully 3D printed directly without the use of any additional support. As this setup creates a curing rate which is of the same rate as the ink’s spreading process, allowing to fix the shape of the trace immediately after extrusion. This is demonstrated by the experiment in section 5.3, where aspect ratio of illuminated traces is up to two times higher than shadowed ones.

7.2 Future work

7.2.1.Integration of mixing

While printing of three inks of different properties have been demonstrated, it would be advantageous to develop the printhead further such that it allows mixing of ink ingredients in variable ratios to produce an ink with the required properties on demand. The low viscosity of the inks used in the research makes them ideally suited for mixing. Instead of using discrete inks which include all components of the final cured polymer such as base, cross linker, chain extender and color, each of them can become a separately stored ink ingredient which would be delivered to a micromixer in the selected ratio to the others. The mixed ink can then be deposited and cured similarly to the current method. Such a capability would enable creation of a variable array of final material qualities such as hardness and color from a small set or precursor materials.

7.2.2.Surface modifications

Though the printer has been used to print objects out of silicone ‘building’ inks, the resulting part has the same properties throughout the volume of each deposited ink. It would be interesting to add a secondary chemical treatment capability once the part is printed. For example, an addition of surface modification reagents which are applied to the printed object’s surface to functionalize it only in the selected areas. Such treatments can include treating the surface to be more hydrophilic, or priming the surface for better adhesion to other materials (as silicone is notoriously difficult to bond).

7.2.3.Over printing

Another promising avenue of exploration is to develop the capability to ‘over-print’ silicone over existing objects. The conformal nature of the low viscosity inks, allows them to wet and conform fully to the underlying surface features. these inks can be applied as a separate step in the object’s manufacturing or treatment rather than as the base of the object. An interesting application of such a capability is adding a layer of silicone inks as a damping material in the manufacturing of bone replacement implants or as a bio-inert coating to any other type of implant.

References

[1] Femmer, T., Kuehne, a, & Wessling, M. (2014). Print your own membrane: Direct rapid prototyping of polydimethylsiloxane. Lab on a Chip, 14, 2610–2613. https://doi.org/10.1039/c4lc00320a

[2] Rekštytė, S., Malinauskas, M., & Juodkazis, S. (2013). Three-dimensional laser micro-sculpturing of silicone: towards bio-compatible scaffolds. Optics Express, 21(14), 17028. https://doi.org/10.1364/OE.21.017028

[3] Liravi, F., Darleux, R., Toyserkani, E., Liravi, F., Darleux, R., & Toyserkani, E. (2015). Nozzle dispensing additive manufacturing of polysiloxane : dimensional control. J . Rapid Manufacturing Int . J . Rapid Manufacturing, 5(Y), 20–43. https://doi.org/10.1504/IJRAPIDM.2015.073546

[4] Hinton, T. J., Hudson, A., Pusch, K., Lee, A., & Feinberg, A. W. (2016). 3D Printing PDMS Elastomer in a Hydrophilic Support Bath via Freeform Reversible Embedding. ACS Biomaterials Science and Engineering, 2(10), 1781–1786. https://doi.org/10.1021/acsbiomaterials.6b00170

[5] O'Bryan, C. S., Bhattacharjee, T., Hart, S., Kabb, C. P., Schulze, K. D., Chilakala, I., … Angelini, T. E. (2017). Self-assembled micro-organogels for 3D printing silicone structures. Science Advances, 3(5), e1602800. https://doi.org/10.1126/sciadv.1602800

[6] Wacker Chemie AG. (2015). Printing with Silicones Building 3D Objects Layer by Layer, 14.

[7] mire, Charles, Finkle, andrew, castel, M. (2015). US20170190118A1. US.

[8] Lee, J., Kim, K. E., Bang, S., Noh, I., & Lee, C. (2017). A desktop multi-material 3D bio-printing system with open-source hardware and software. International Journal of Precision Engineering and Manufacturing, 18(4), 605–612. https://doi.org/10.1007/s12541-017-0072-x

[9] http://bioprinting.aether1.com

[10] Hardin, J. O., Ober, T. J., Valentine, A. D., & Lewis, J. A. (2015). Microfluidic printheads for multimaterial 3D printing of viscoelastic inks. Advanced Materials, 27(21), 3279–3284. https://doi.org/10.1002/adma.201500222

[11] Schneider, F., Draheim, J., Kamberger, R., & Wallrabe, U. (2009). Process and material properties of polydimethylsiloxane (PDMS) for Optical MEMS. Sensors and Actuators A: Physical, 151(2), 95–99. https://doi.org/https://doi.org/10.1016/j.sna.2009.01.026

[12] Belanger, M. C., & Marois, Y. (2001). Hemocompatibility, biocompatibility, inflammatory and in vivo studies of primary reference materials low-density polyethylene and polydimethylsiloxane: a review. Journal of Biomedical Materials Research, 58(5), 467–477.

[13] Charati, S. G., & Stern, S. A. (1998). Diffusion of Gases in Silicone Polymers: Molecular Dynamics Simulations. Macromolecules, 31(16), 5529–5535. https://doi.org/10.1021/ma980387e

[14] Graiver, D., Farminer, K. W., & Narayan, R. (2003). A Review of the Fate and Effects of Silicones in the Environment. Journal of Polymers and the Environment, 11(4), 129–136. https://doi.org/10.1023/A:1026056129717

[15] Williams, D. F. (2008). On the mechanisms of biocompatibility. BIOMATERIALS, 29(20), 2941–2953. https://doi.org/10.1016/j.biomaterials.2008.04.023

[16] McDonald, J. C., & Whitesides, G. M. (2002). Poly(dimethylsiloxane) as a Material for Fabricating Microfluidic Devices. Accounts of Chemical Research, 35(7), 491–499. https://doi.org/10.1021/ar010110q

[17] Palchesko, R. N., Zhang, L., Sun, Y., & Feinberg, A. W. (2012). Development of Polydimethylsiloxane Substrates with Tunable Elastic Modulus to Study Cell Mechanobiology in Muscle and Nerve. PLoS ONE, 7(12). https://doi.org/10.1371/journal.pone.0051499

[18] Kim, D.-H., Ghaffari, R., Lu, N., & Rogers, J. A. (2012). Flexible and Stretchable Electronics for Biointegrated Devices. Annual Review of Biomedical Engineering, 14(1), 113–128. https://doi.org/10.1146/annurev-bioeng-071811-150018

[19] https://www.okuma.com/genos-m460-ve

[20] "Sylgard® 184 Silicone Elastomer Product Information" http://www.dowcorning.com/DataFiles/090276fe80190b08.pdf Accessed 5.8.17

[21] Delivopoulos, E., Minev, I. R., & Lacour, S. P. (2011). Evaluation of negative photo-patternable PDMS for the encapsulation of neural electrodes. 2011 5th International IEEE/EMBS Conference on Neural Engineering, NER 2011, 490–494. https://doi.org/10.1109/NER.2011.5910593

[22] Chemical Co, A. (n.d.). Aldrich Polymer Products Applicaton Reference Information, (1), 5–19.

[23] http://www.ldgi.com/zh/wp-content/uploads/sites/2/LDGI-OmniCure-S1000-Brochure.pdf , accessed 3.11.17

[24] BASF document. (n.d.). High lights! Radiation curing with resins and photoinitiators for industrial coatings and graphic arts: Laromer, Irgacure, Lucirin, Darocur. Retrieved from https://www.basf.com/group/corporate/de/literature-document:/Brand+Darocur-Brochure--High+lights+Radiation+curing+with+resins+and+photoinitiators+for+industrial+coatings+and+graphic+arts+Laromer+Irgacure+Lucirin+Darocur-English.pdf ,accessed 09.06.16

[25] Bradski, G. (2000). The OpenCV Library. Dr. Dobb's Journal of Software Tools.

[26] Rueden, C. T.; Schindelin, J. & Hiner, M. C. et al. (2017), "ImageJ2: ImageJ for the next generation of scientific image data", BMC Bioinformatics 18:529, doi:10.1186/s12859-017-1934-z.

[27] thecooltool, "The NEW modular UNIMAT 3D-PRINTER-System", http://www.thecooltool.com/uploads/media/Unimat_3D-Drucker_WEB.pdf

[28] Silicone. (2016). In: Encyclopædia Britannica. Encyclopædia Britannica, inc., p.https://www.britannica.com/science/silicone.

[29] Rettig, L. A., Luca, L., & Murphy, M. S. (2005). Silicone implant arthroplasty in patients with idiopathic osteoarthritis of the metacarpophalangeal

joint. The Journal of Hand Surgery, 30(4), 667–672. https://doi.org/10.1016/j.jhsa.2005.02.011

[30] Chen, J., Zhou, Y., Wang, D., He, F., Rotello, V. M., Carter, K. R., … Nugen, S. R. (2015). UV-nanoimprint lithography as a tool to develop flexible microfluidic devices for electrochemical detection. Lab Chip, 15, 3086–3094. https://doi.org/10.1039/C5LC00515A

[31] Thangawng, A. L., Ruoff, R. S., Swartz, M. A., & Glucksberg, M. R. (2007). An ultra-thin PDMS membrane as a bio/micro--nano interface: fabrication and characterization. Biomedical Microdevices, 9(4), 587–595. https://doi.org/10.1007/s10544-007-9070-6

[32] Johnston, I. D., McCluskey, D. K., Tan, C. K. L., & Tracey, M. C. (2014). Mechanical characterization of bulk Sylgard 184 for microfluidics and microengineering. Journal of Micromechanics and Microengineering, 24(3). https://doi.org/10.1088/0960-1317/24/3/035017

[33] Janusziewicz, R.; Tumbleston, J.; Quintanilla, A. L.; Mecham, S. J.; DeSimone, J. (2016) Layerless fabrication with continuous liquid interface production; M. Proc. Natl. Acad. Sci. U.S.A. 113(42), 11703-11708.

[34] "Silicone Elastomers Market." [Online]. Available: www.marketsandmarkets.com/PressReleases/silicone-elastomers.asp.

Appendix A, Flowrate experiment data:

Flowrate fits, given are the polynomial coefficients for the equation $Q = \sum_{i=0}^{n} c_i P^i$

Needle Gauge and ink	Fit order 1 in m^3/pa	Fit order 2 in m^3/pa
(22, 'V21H')	3.77e-13, -2.28e-10	1.37e-19, 3.08e-13, -3.92-11
(22, 'V31H')	8.07e-14, -9.00e-12	3.63e-21, 7.89e-14, -3.99e-12
(22, 'V35H')	1.60e-14, -3.60e-12	2.01e-21, 1.50e-14, -8.32e-13
(25, 'V21H')	3.760e-14, -1.21e-1	8.70e-20, -6.11e-15, -1.22e-12
(25, 'V31H')	1.06e-14, -1.4e-11	1.46e-20, 3.2e-15, 5.44e-12
(25, 'V35H')	2.70e-15, -3.31e-12	3.50e-21, 9.44e-16, 1.51e-12

Appendix B, Computer vision code:

The algorithm processes individual image files.

For every file in a specified path do the following.

1. Open,read into image var.
2. Take only Blue channel.
3. Gaussian blur, Canny edge detection, erode and dilate a number of times.
4. At this point, most of the noise has been removed and a central contour is revealed.
5. Collect the largest contour using contour detection, and discarding anything but the biggest contour, by area sorting.
6. Find the rotation of the image by a rotation optimization search.
7. Rotate original image and repeat all above steps again on the rotated image.

   At this point, the Image is in the same state as Fig B1

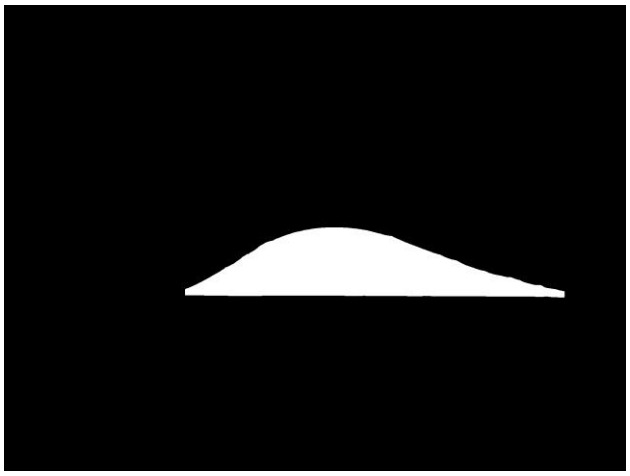

Figure B.1.An image of the same trace as in Figure 3.6, the resulting B/W image after all operations and rotations.

8. Enclose with box[6] and measure box dimensions. measure area and moments of the trace shape, relative to its aligned axes[7].

[6] The rotation followed by a box cannot be replaced by smallest enclosing box algorithm, as it is often not aligned to the horizontal width direction.

9. Superimpose a box and horizon detection on the original image with 0.5alpha resulting in the image in figure 2.8.
10. Collect all the above data for all scanned traces in a single report.

This algorithm allowed to rapidly analyze the large set of images generated.

```
from __future__ import division

import numpy as np
import argparse
import imutils
import cv2
import cv
import math
import os
import csv
import image_operations.service as im_service
import image_operations.rotate as im_rotate
import traceback
import re
#service functions
def box_to_points(x,y,w,h):
    return((x,y),(x+w,y),(x+w,y+h),(x,y+h))

def show_image(image):
    cv2.namedWindow('dst_rt', cv2.WINDOW_NORMAL)
    cv2.resizeWindow('dst_rt', 640, 480)
    cv2.imshow('dst_rt', image)
    cv2.waitKey(0)
    cv2.destroyAllWindows()

def find_biggest_contour(contours):
    maxsize=0
    maxcontour,i=None,None
    for i,contour in enumerate(contours):
        if cv2.contourArea(contour)>maxsize:
            maxsize=cv2.contourArea(contour)
            maxcontour=contour
    return maxcontour,i

def raw_moment(data, iord, jord):
    nrows, ncols = data.shape
    y, x = np.mgrid[:nrows, :ncols]
    data = data * x**iord * y**jord
    return data.sum()

def variance_of_laplacian(image):
    # compute the Laplacian of the image and then return the focus
    # measure, which is simply the variance of the Laplacian
    return cv2.Laplacian(image, cv2.CV_64F).var()


class Processed_trace_image():
    def __init__(self,image):
        self.imgs={}
        self.imgs['image']=image
        self.info={}
        self.height,self.width=self.imgs['image'].shape[:2]
```

[7] The X and Y axes after rotation

```
    def rotation(self):
        self.imgs["trace_outline"] =
self.get_largest_contour(self.imgs['trace_shape'].copy(), filled=8)

        self.imgs['framed'] = im_service.add_frame(self.imgs["trace_outline"])

self.imgs["resized"]=imutils.resize(self.imgs['framed'],int(self.width/10),int(sel
f.height/10))
        #im_service.show_image(self.imgs["resized"])
        results = im_rotate.Rotate_by_fitness_search(self.imgs["resized"], lambda
x:im_rotate.sum_x_lines_powers(x, 25), np.arange(-45,45,0.25))
        self.imgs["rotated_trace"]=results[-1]
        self.rotation_angle=results[1]
        #im_service.show_image(results[-1])
        return results[1]


    def process(self):

        self.imgs['edged'] = self.rough_outline(self.imgs['image'].copy())
        self.process_trace()
        self.calculations()

    def process_trace(self):

        self.imgs['trace_shape'] =
self.get_largest_contour(self.imgs['edged'].copy())

        self.imgs['trace_shape'] = cv2.GaussianBlur(self.imgs['trace_shape'], (9,
9), 0)
        retval,self.imgs['trace_shape']= cv2.threshold(self.imgs['trace_shape'],
127, 255, cv2.THRESH_BINARY)

        smaller_contour = cv2.erode(self.imgs['trace_shape'],
np.ones((5,5),np.uint8), iterations=5)
        dilated_contour=cv2.dilate(smaller_contour, np.ones((5,5),np.uint8),
iterations=5)
        self.imgs['trace_shape'] = self.get_largest_contour(dilated_contour)
        self.trace_contour =
self.get_largest_contour(self.imgs['trace_shape'].copy(), get_contour=True)

        self.imgs['trace_shape'] = cv2.GaussianBlur(self.imgs['trace_shape'], (9,
9), 0)
        retval,self.imgs['trace_shape']= cv2.threshold(self.imgs['trace_shape'],
127, 255, cv2.THRESH_BINARY)

        self.trace_contour =
self.get_largest_contour(self.imgs['trace_shape'].copy(), get_contour=True)

    def calculations(self):
        self.I = {"m00":raw_moment(self.imgs['trace_shape'], 0, 0),
             "m01":raw_moment(self.imgs['trace_shape'], 0, 1),
             "m10":raw_moment(self.imgs['trace_shape'], 1, 0),
             "m11":raw_moment(self.imgs['trace_shape'], 1, 1)}

        self.cx =self.I['m01'] / self.I['m00']
        self.cy = self.I['m10'] / self.I['m00']

        self.box = tuple(cv2.boundingRect(self.trace_contour))
        self.boxpts =box_to_points(*self.box)
        self.boxpts = np.int0(self.boxpts)

    def get_properties(self):

        self.info['width']=self.box[2]
        self.info['height'] = self.box[3]
        self.info.update(self.I)
```

```
        return self.info

    def get_composite(self):
        cnt = cv2.cvtColor(self.imgs['trace_shape'], cv2.COLOR_GRAY2RGB)
        self.imgs['composite_image'] = (cv2.addWeighted(self.imgs['image'], 0.6,
cnt, 0.4, 0.0))
        cv2.circle(self.imgs['composite_image'], (int(self.cx), int(self.cy)), 10,
(255, 0, 0), thickness=-1)
        #cv2.line(self.imgs['composite_image'], (0, int(self.divider.y(0))),
(self.width - 1, int(self.divider.y(self.width - 1))), (0, 255, 0), 4)
        cv2.drawContours(self.imgs['composite_image'], [self.boxpts], 0, (0, 0,
255), 3)
        return self.imgs['composite_image']

    def rough_outline(self,image):
        self.imgs['gray'] = cv2.split(image)[0].copy()
        # perform edge detection, then perform a dilation + erosion to
        # close gaps in between object edges
        self.sharpness=variance_of_laplacian(self.imgs['gray'])
        self.info["sharpness"]=self.sharpness
        self.imgs['gray_blurred'] = cv2.GaussianBlur(self.imgs['gray'], (31, 31),0)
        self.imgs['edged'] = cv2.Canny(self.imgs['gray_blurred'], 1000, 2000,
apertureSize=7, L2gradient=True)
        self.imgs['dilated'] = cv2.dilate(self.imgs['edged'] , None, iterations=5)
        self.imgs['eroded'] = cv2.erode(self.imgs['dilated'], None, iterations=3)
        return self.imgs['eroded']

    def get_largest_contour(self, bw_img, get_contour=False,filled=-1):
        contours, hierarchy = cv2.findContours(bw_img, cv2.RETR_LIST,
cv2.CHAIN_APPROX_NONE)
        biggest_contour, i = find_biggest_contour(contours)
        if get_contour:
            return biggest_contour
        # make empty image to superimpose contour
        empty = np.zeros(bw_img.shape[:2], np.uint8)
        cv2.drawContours(empty, [biggest_contour], 0, (255), filled)
        return empty



def main():
    print("Executing trace resoultion Computer vision script")
    """should return a dictionary with properties to use later"""
    # construct the argument parse and parse the arguments
    ap = argparse.ArgumentParser()
    ap.add_argument("-i", "--images_folder", required=True,
                    help="path to the input image folder")
    ap.add_argument("-r", "--report", required=True,
                    help="path to the report")
    ap.add_argument("-b", "--bw_output", required=True,
                    help="path to the bw output folder")
    ap.add_argument("-c", "--composite_output", required=True,
                    help="path to the composite output folder")

    args = vars(ap.parse_args())

    csv_file=open(args['report'], 'wb')
    writer = csv.writer(csv_file)
    first=True
    for dirname, dirnames, filenames in os.walk(args['images_folder']):
        for filename in filenames:
            if filename.endswith(('.dpx', '.jpg', '.jpeg', '.exr', '.tif')):
                print("Working on "+os.path.join(dirname,filename))
                image_name=filename.split(".")[0]
                image = cv2.imread(os.path.join(dirname,filename))
                try:
```

```
                    Trace=Processed_trace_image(image)
                    Trace.name=filename

                    Trace.process()
                    angle=Trace.rotation()
                    M = cv2.getRotationMatrix2D((Trace.cx , Trace.cy), angle, 1)
                    rotated_image = cv2.warpAffine(image, M, (Trace.width,
Trace.height))
                    Trace = Processed_trace_image(rotated_image)
                    Trace.process()

                except Exception as e:
                    traceback.print_exc()
                    continue

cv2.imwrite(os.path.join(args['composite_output'],image_name+'.tif'),Trace.get_com
posite())
                cv2.imwrite(os.path.join(args['bw_output'] , image_name + '.tif'),
Trace.imgs['trace_shape'])
                properties=Trace.get_properties()
                if first:
                    writer.writerow(['filename']+sorted(properties.keys()))
                    first=False

                summary=[os.path.join(dirname,filename)]+[properties[k] for k in
sorted(properties.keys())]
                print(str(summary))
                writer.writerow(summary)


if __name__ == "__main__":
    main()

-----------------------------
```